IEEE Access
Multidisciplinary ⋮ Rapid Review ⋮ Open Access Journal

Received October 15, 2021, accepted November 17, 2021, date of publication December 3, 2021, date of current version January 31, 2022.

Digital Object Identifier 10.1109/ACCESS.2021.3132802

Fault-Tolerant, Distributed Control for Emerging, VSC-Based, Islanded Microgrids– An Approach Based on Simultaneous Passive Fault Detection

MOHAMMAD RAEISPOUR[1], HAJAR ATRIANFAR[1], (Member, IEEE), MASOUD DAVARI[2], (Senior Member, IEEE), AND GEVORK B. GHAREHPETIAN[1], (Senior Member, IEEE)

[1]Department of Electrical Engineering, Amirkabir University of Technology (Tehran Polytechnic), Tehran 1591634311, Iran
[2]Department of Electrical and Computer Engineering, Allen E. Paulson College of Engineering and Computing, Georgia Southern University at Statesboro, Statesboro, GA 30460, USA

Corresponding author: Masoud Davari (mdavari@georgiasouthern.edu; davari@ualberta.ca)

The work of Masoud Davari was supported by the U.S. National Science Foundation (U.S. NSF) under ECCS-EPCN Awards #1808279 and #1902787 granted by the U.S. NSF core program of Energy, Power, Control, and Networks (EPCN) in the Division of Electrical, Communications and Cyber Systems (ECCS), as well as the professional development part of his 2020-2021 Discovery & Innovation Award from the University Awards of Excellence at Georgia Southern University—the funding by the U.S. NSF ECCS-EPCN is greatly acknowledged by Masoud Davari. The work of Gevork B. Gharehpetian was supported by the Iran National Science Foundation (INSF) under project No. 96005975—the funding by INSF is greatly acknowledged by Gevork B. Gharehpetian. This work was also supported in part by dSPACE GmbH Company, SEMIKRON Company, and Verivolt Company for the Laboratory for Advanced Power and Energy Systems (LAPES)—where the experiments of this research were entirely conducted and where Masoud Davari has founded, established, and directed at Georgia Southern University.

ABSTRACT This paper proposes a fault-tolerant control and a robust, distributed, simultaneous, passive fault detection and isolation (or FDI) for islanded ac microgrids (MGs), including heterogeneous distributed generations and battery energy storage systems (BESSs). Disturbances and both actuator and sensor faults are considered in this paper to design a robust distributed control. The nature of the considered faults is general to deal with any sources, e.g., cyber threats (in the form of data integrity attacks) and sensor issues. In this regard, a mixed H_∞/H_- formulation is introduced in order to detect and eliminate the undesirable effects of the aforementioned defected components simultaneously, thereby achieving robust performance. Besides, sufficient conditions based on extended linear matrix inequality (also known as LMI) are outlined. Voltage and frequency regulation, active power-sharing, and the state of charge balance of BESSs under faulty conditions are investigated. Different scenarios are tested on a detailed model of a test MG system. The effectiveness of the proposed scheme on mitigating the impacts of faults and disturbances on the distributed energy resources' (DERs') performance is evaluated through comprehensive and comparative simulations based on MATLAB/Simulink. Moreover, experimental studies are conducted in order to validate the results in the corresponding practical scenarios.

INDEX TERMS Distributed control, fault-tolerant, fault detection and isolation, linear matrix inequality, islanded microgrid, mixed H_∞/H_- optimization, voltage-source converter (VSC).

I. INTRODUCTION

Microgrids (MGs) can operate in either islanded (equivalently off-grid) or grid-connected mode. In the islanded mode, MGs' control system should balance supply and demand via power-sharing control and maintain the stability and synchronization on voltage and frequency. In grid-connected mode, voltage and frequency are dictated by the upstream utility grid, and the basic control objectives of grid-connected mode are control of transferred active and reactive powers and meeting the power quality standard requirements [1]–[5]. Hierarchical control structure—including the primary, secondary, and tertiary layers—has widely been used to control MGs. In the primary layer, droop control sustains the frequency and voltage in an admissible span and realizes the basic power-sharing [6]. These operations are based on local

The associate editor coordinating the review of this manuscript and approving it for publication was S. K. Panda.

measurements and do not need external communications. Also, advanced techniques such as robust sliding mode control (SMC) [7], robust mixed H_2/H_∞ output feedback control [8], model predictive control [9], and robust nonlinear control strategies [10], [11], have been proposed according to droop and non-droop manners in the primary layer.

The secondary layer should compensate for the steady-state errors of frequency and voltage due to the primary control [12], [13]. In contrast, the tertiary control level's main task is power flow optimization and unit commitment [14], [15]. Lately, various features of distributed secondary control of MG such as fixed-time communication delays [16], event-triggered control [17], nonuniform time-varying communication delays [18], resiliency to relative state-dependent noises [19], resiliency to uncertain communications [20], resilient synchronization of voltage/frequency under deception attacks [21], the resilient H_∞ consensus-based control for uncertain time-delayed communication [13] have been addressed in the literature. In the reported studies, one of the critical aspects which have been less considered is fault detection and isolation (commonly known as FDI) and ''fault-tolerability.'' Regarding MG's natural construction, the sensors/actuator have to be extended in unattended environments. This matter constitutes a significant challenge in offering a good quality of service. Faults could occur in different components of the systems including sensors, actuators, or even in communication networks. Therefore, it is indispensable to accommodate them in an effective resilient fault-tolerant control strategy in order to hinder further failures.

Among the existing research on the fault-tolerant control in power systems, [22], [23] have discussed the sensor faults based on unknown input observer methods for the load frequency control. These studies have been performed in a centralized manner. Also, in case of faults in MGs, [24] has presented a robust protocol based on sliding mode fault resilient control using a distributed approach. Recently in [25], a cooperative fault-tolerant control has been suggested for the scenario in which the topology of the network is time-varying. These studies have solely considered actuator faults in MGs. In [26], the authors have investigated the impact of sensor faults on the MG as a model of false date injection attack, which are unknown and bounded. In [27], [28], a distributed fault-tolerant control algorithm for the restoration of voltage and frequency in islanded ac MGs has been addressed, and sensor/actuator faults have been considered.

However, all the existing methods still have three significant drawbacks that limit their performance in real applications; 1) The present methodologies for fault-tolerant control are mainly based on the SMC, which despite its simplicity, has the dilemma of non-convergence in finite time, and steady-state error and the need for the prior information of the upper bound value of uncertainties and disturbances. 2) In the current approaches, a controller and at least one estimator are employed for each unit. Therefore, if the number of distributed energy resources (DERs) increases, their implementation becomes very complicated and, in some cases, impossible. 3) The methods investigating the faults in the secondary layer of MG are based on fault-tolerant control and have not discussed FDI. Therefore, these approaches cannot address possible faults in the secondary layer.

In this paper, a robust distributed simultaneous passive FDI, and fault-tolerant control have been proposed in order to tackle all of the mentioned drawbacks for real applications in islanded ac MGs. The main contributions of this paper are:

1) A robust, LMI-based approach to the mixed H_∞/H_- is proposed for simultaneous FDI and fault-tolerant control. In this method, based on the residual signals and the control signal, a control algorithm is proposed for the MG secondary layer. Accordingly, the fault in each agent and the fault in the neighboring agents can be detected. The way that the faults are considered in this research can cover a wide variety of sources, such as cyberattacks (e.g., data integrity attacks), sensor-related problems, and so forth.
2) In order to guarantee the team's faulty DER isolation, a satisfactory condition on the network topology and residual signals is necessary to be obtained. It is based on flags generated and corresponding to residual signals of the team DERs.
3) In order to reduce the computational complexity and to facilitate the implementation, the system dynamics are decomposed to a set of first-order subsystems. Finally, an extended LMI formulation is used to avoid using standard Lyapunov variables.

The rest of this paper is organized as follows. Section II describes the preliminaries of graph theory and some notation, and dynamic modeling of MG. The proposed robust distributed FDI and fault-tolerant voltage and frequency regulation, providing active power-sharing, and state of charge (SOC) balance are presented in Section III. The performance verification of the proposed control strategy by simulations and comparison with other reported methods is provided in Section IV. Section V displays some experimental results to show the proposed methodology's effectiveness. Finally, Section VI concludes this research.

II. PRELIMINARIES AND PROBLEM FORMULATION

A. GRAPH THEORY AND NOTATION

The communication topology among DERs are modeled by an undirected graph $\mathcal{G} = (\mathcal{V}, \mathcal{E})$, where the set of nodes (according to each DERs) is $\mathcal{V} = \{v_i : i \in N\}$, and $N = \{1, 2, \ldots, n\}$. $\mathcal{E} \subseteq \mathcal{V} \times \mathcal{V}$ is the set of edges. The set of neighbors of node v_i is denoted by $N_i = \{v_j \in \mathcal{V} : (v_j, v_i) \in \mathcal{E}\}$. The graph Laplacian matrix $\mathcal{L}_G = [l_{ij}] \in R^{n\times n}$ is defined by $l_{ii} = |N_i|$, $l_{ij} = 0$ where $j \notin N_i$, and $l_{ij} = -1$ where $j \in N_i$. Throughout this paper, $\otimes$ denotes the Kronecker product of matrices, the Hermitian part of a square matrix A is denoted by $Herm(A) = A + A^T$ and $T_{xy}(s)$ denotes the transfer matrix from y to x. The H_∞ norm, H_- index and

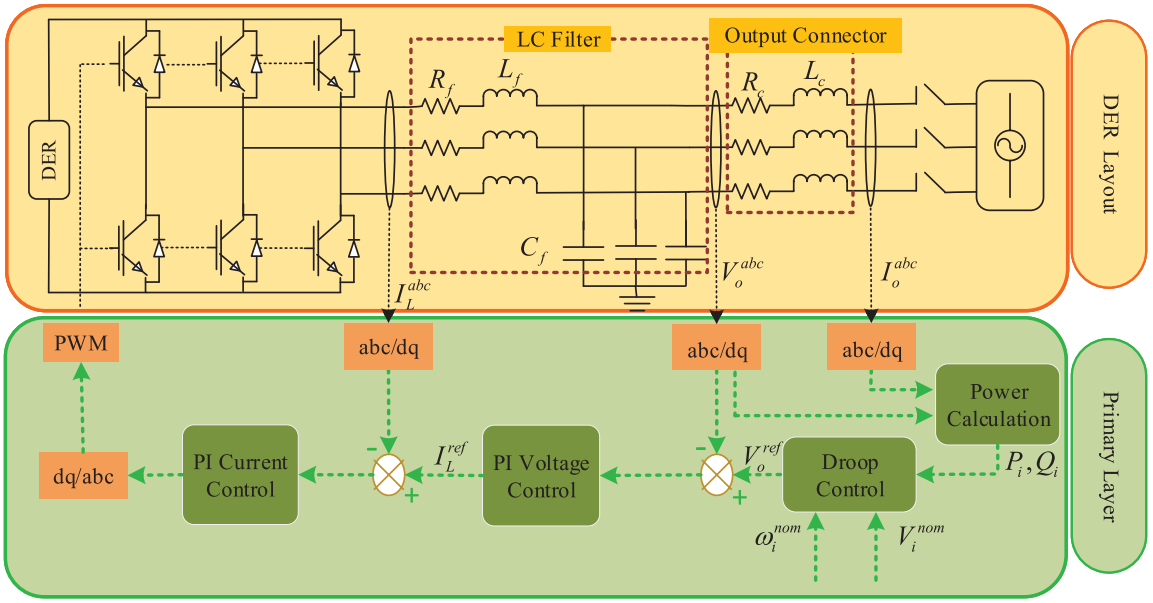

FIGURE 1. Microgrid's primary layer schematic.

H_-^+ index of $T(s)$ are defined as $\|T\|_\infty = \sup_{\omega\in\Re}\bar{\sigma}(T(j\omega))$, $\|T\|_- = \inf_{\omega\in\Re}\underline{\sigma}(T(j\omega))$ and $\|T\|_-^+ = \inf_{\omega\in\Re}\underline{\sigma}^+(T(j\omega))$, respectively, where $\bar{\sigma}$, $\underline{\sigma}$ and $\underline{\sigma}^+$ denote the maximum, the minimum and the minimum nonzero singular values of $T(s)$, respectively.

B. DYNAMIC MODELING OF MICROGRID

The first step toward designing control algorithms in dynamic systems is to mathematically model their behavior using differential and algebraic equations. In this regard, the dynamic equations of the output connectors and LCL filters are acquired to tune the voltage and current controller's parameters in the primary layer [7]. This study aims to design a proper, distributed control algorithm for the secondary layer of islanded MGs. The droop equations are usually used to relate the primary and secondary layers in hierarchical-based MG systems. The voltage and frequency droop equations for distributed generations (DG) units can be written as

$$\begin{cases} \omega_i = \omega_i^{\text{nom}} - m_i^P P_i \\ V_{\text{odi}} = V_i^{\text{nom}} - n_i^Q Q_i \\ V_{oqi} = 0 \end{cases} \tag{1}$$

where ω_i, V_{odi} and V_{oqi} are respectively frequency, direct and quadratic components of output voltage of i^{th} unit, P_i and Q_i are low-pass filtered values of the i^{th} unit active and reactive power, as the same way, m_i^P, n_i^Q are constant active and reactive power droop factor, respectively. Also, V_i^{nom} and ω_i^{nom} are the voltage and frequency setpoints applied by the secondary layer Fig. 1.

Considering the importance of battery energy storage systems (BESSs) charge level and impacts of SOCs on the proportional active power-sharing among DER units, it is necessary to provide a modified frequency droop equation to operate BESS units in islanded operations. The modified droop equation can be expressed as

$$\omega_i = \omega_i^{\text{nom}} - m_i^P P_i - k_i^{\overline{\text{SoC}}}\overline{SoC_i} \tag{2}$$

where $\overline{SoC_i}$ is SOC complement of the i^{th} BESS and $k_i^{\overline{\text{SoC}}}$ is the droop factor of the i^{th} BESS. More details regarding the equation, as mentioned above, and its properties can be obtained from [29]. Now, it is required to calculate the derivatives of the mentioned droop equations to design distributed secondary control algorithms for the islanded operation of DG and BESS units. The secondary protocols can be designed using the following equations:

$$\begin{cases} \dot{V}_i^{\text{nom}} = u_i^v + u_i^Q \\ \begin{cases} \dot{\omega}_i^{\text{nom}} = u_i^\omega + u_i^P & DER_i \in DG \\ \dot{\omega}_i^{\text{nom}} = u_i^\omega + u_i^P + u_i^{\overline{\text{SoC}}} & DER_i \in BESS \end{cases} \end{cases} \tag{3}$$

where $u_i^P = m_i^P \dot{P}_i$, $u_i^Q = n_i^Q \dot{Q}_i$, $u_i^{\overline{\text{SoC}}} = k_i^{\overline{\text{SoC}}}\dot{\overline{SoC}}_i$, $u_i^v = \dot{V}_{\text{odi}}$ and $u_i^\omega = \dot{\omega}_i$ denote the active power, reactive power, SOC balance, voltage and frequency control signals, respectively.

III. MAIN RESULTS

A. ROBUST DISTRIBUTED FAULT-TOLERANT ACTIVE POWER-SHARING AND SOC BALANCE

In this section, the principal objective is to design a control law such that the active power-sharing and a SOC balance of DERs could be attained. In addition to these objectives, the controller should guarantee the stability and robustness of the system in the presence of disturbances, and actuator/sensor faults. The layout of the secondary layer is demonstrated in Fig. 2. Besides, the consensus protocol must be designed to

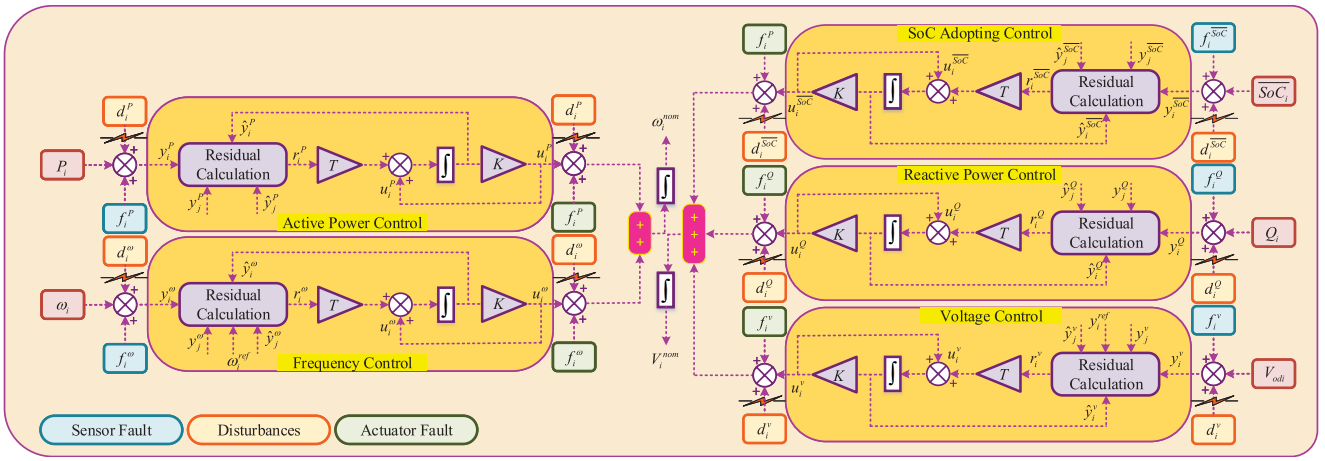

FIGURE 2. Microgrid's secondary layers schematic.

meet the following properties.

$$\begin{cases} m_1^P P_1(t) = \ldots = m_n^P P_n(t) \\ n_1^Q Q_1(t) = \ldots = n_n^Q Q_n(t) \\ k_1^{\overline{\text{SoC}}}\, \overline{SoC}_1(t) = \ldots = k_n^{\overline{\text{SoC}}}\, \overline{SoC}_n(t) \end{cases} \tag{4}$$

Without loss of generality, by considering the faults and disturbances in dynamics of the system, the following equation is expressed for powers and SOCs of DERs:

$$\begin{cases} \dot{\zeta}_i(t) = B_u u_i(t) + B_d d_i(t) + B_f f_i(t) \\ y_i(t) = C\zeta_i(t) + D_d d_i(t) + D_f f_i(t) \end{cases} \tag{5}$$

where $\zeta_i(t) = (m_i^P P_i(t), n_i^Q Q_i(t), k_i^{\overline{\text{SoC}}} \overline{SoC}_i(t))^T$ denotes the state vector, $u_i(t) = (u_i^P, u_i^Q, u_i^{\overline{\text{SoC}}})^T$ represents the control input vector, $d_i(t) = (d_i^P, d_i^Q, d_i^{\overline{\text{SoC}}})^T$ is an L_2-norm bounded signal that represents unmodeled dynamics of the ith DERs, including unknown disturbances and uncertainties and $f_i(t) = (f_i^P, f_i^Q, f_i^{\overline{\text{SoC}}})^T$ represents the fault signals. B_u is the input matrix, C is the output matrix, B_d, D_d expresses input and output disturbance matrices, respectively, and B_f, D_f denote input and output fault matrices, respectively. The superscripts P, Q, and $\overline{SoC}$ correspond to active power, reactive power, and SOC, respectively. To combine relative information and achieve consensus as defined in (4), the controlled output function is specified as

$$\begin{cases} z_i^P(t) = m_i^P.P_i(t) - \dfrac{1}{n}\displaystyle\sum_{j=1}^{n} m_j^P.P_j(t) \\ z_i^Q(t) = n_i^Q.Q_i(t) - \dfrac{1}{n}\displaystyle\sum_{j=1}^{n} n_j^Q.Q_j(t) \\ z_i^{\overline{\text{SoC}}}(t) = k_i^{\overline{\text{SoC}}}.\overline{SoC}_i(t) - \dfrac{1}{n}\displaystyle\sum_{j=1}^{n} k_j^{\overline{\text{SoC}}}.\overline{SoC}_j(t) \end{cases} \tag{6}$$

where the vector $z_i = (z_i^P, z_i^Q, z_i^{\overline{\text{SoC}}})^T$ denotes the relative information of ith DER. To achieve this goal, the following FDI filter is considered.

$$\begin{cases} \dot{\hat{\zeta}}_i(t) = B_u u_i(t) + T r_i(t) \\ u_i(t) = K\hat{\zeta}_i(t) \\ r_i(t) = \xi_i(t) - \hat{\xi}_i(t) \end{cases} \tag{7}$$

where $\hat{\zeta}_i(t)$ represents the observer states vector, $r_i(t)$ represents the residual signal, and T and K matrices denote the filter gains to be selected and specified subsequently. Moreover, $\xi_i(t) = \sum_{j\in N_i}(y_i(t) - y_j(t))$ generates the relative output information and $\hat{\xi}_i(t) = \sum_{j\in N_i} C(\hat{\zeta}_i(t) - \hat{\zeta}_j(t))$. By incorporation the equations (5) and (7), the following closed-loop dynamic is derived.

$$\begin{cases} \dot{\zeta}_{\text{cl}} = A_{\text{cl}}\zeta_{\text{cl}}(t) + B_{\text{dcl}}D(t) + B_{\text{fcl}}F(t) \\ R(t) = C_{\text{cl}}\zeta_{\text{cl}}(t) + D_{\text{dcl}}D(t) + D_{\text{fcl}}F(t) \\ Z(t) = \widehat{C}_{\text{cl}}\zeta_{\text{cl}}(t) \end{cases} \tag{8}$$

where the variable are as $e_i = \zeta_i - \hat{\zeta}_i$, $e = [e_1^T, \ldots, e_n^T]^T$, $\zeta = [\zeta_1^T, \ldots, \zeta_n^T]^T$, $\hat{\zeta} = [\hat{\zeta}_1^T, \ldots, \hat{\zeta}_n^T]^T$, $D = [d_1^T, \ldots, d_n^T]^T$, $R = [r_1^T, \ldots, r_n^T]^T$, $Z = [z_1^T, \ldots, z_n^T]^T$ and consequently, the system matrices are reached as

$$\begin{aligned} A_{\text{cl}} &= \begin{bmatrix} -\mathcal{L}\otimes TC & 0 \\ -I\otimes B_u K & I\otimes B_u K \end{bmatrix}, \\ B_{\text{dcl}} &= \begin{bmatrix} I\otimes B_d - \mathcal{L}\otimes TD_d \\ I\otimes B_d \end{bmatrix}, \quad C_{\text{cl}} = \begin{bmatrix} \mathcal{L}\otimes C & 0 \end{bmatrix}, \\ B_{\text{fcl}} &= \begin{bmatrix} I\otimes B_f - \mathcal{L}\otimes TD_f \\ I\otimes B_f \end{bmatrix}, \quad \widehat{C}_{\text{cl}} = \begin{bmatrix} 0 & \mathcal{L}_c\otimes I \end{bmatrix} \end{aligned} \tag{9}$$

It is clear that the state vector corresponds to $\zeta_{\text{cl}} = \begin{bmatrix} e^T & \zeta^T \end{bmatrix}^T$ and $D_{\text{dcl}} = \mathcal{L}\otimes D_d, D_{\text{fcl}} = \mathcal{L}\otimes D_f$. Moreover, $\mathcal{L}$ denotes the Laplacian matrix, and the matrix $\mathcal{L}_c = [l_{c_{ij}}]$ is symmetric and $l_{c_{ij}} = \frac{-1}{n}$ and $l_{c_{ii}} = \frac{n-1}{n}$ for $i \neq j$.

The goal is to design the controller such that, the following objectives are guaranteed.

1) Closed-loop system (8) should be stable.
2) Due to the need for increasing the sensitivity of the system with respect to fault signals in fault detection modules, the effect of them on the residual signal should be maximized, while minimizing the impacts of disturbances.
3) In order to achieve robust performances and fault tolerant control, the effects of disturbances and fault signals on the control outputs should be minimized.

In order to attenuate the effect of disturbances on the residuals and the control outputs—and reduce the control outputs fault's effects—H_∞ norm is employed. Also, to assure the residual high sensitivity to the faults, the H_-^+ index is applied. In order to simultaneously solve the fault detection and fault-tolerant consensus control of active power, reactive power, and an SOC balance, the following optimization problem is considered.

$$\begin{aligned} &\min\ \alpha_1\gamma_1+\alpha_2\gamma_2+\alpha_3\gamma_3-\alpha_4\beta\\ &s.t:\ \|T_{RD}\|_\infty<\gamma_1,\quad \|T_{RF}\|_-^+>\beta,\\ &\qquad \|T_{ZD}\|_\infty<\gamma_2,\quad \|T_{ZF}\|_\infty<\gamma_3 \end{aligned} \tag{10}$$

The positive constant weights $\alpha_1, \alpha_2, \alpha_3$, and α_4 can be used by the designer as a trade-off among the objectives, and $\gamma_1, \gamma_2, \gamma_3, \beta$ are positive scalars. Note that since the Laplacian matrix of the system described in (5) is singular, the matrix $A_{\rm cl}$ is unstable. Without loss of generality, based on Lemma 2 in [30], the Laplacian matrix can be decomposed into two parts, namely agreement and disagreement parts. As far as the computational complexity of the closed-loop system when the number of DERs is high, the implementation of the controller is exceedingly challenging. By reducing the computational complexity of the problem, the closed-loop system can be decomposed into a set of independent decoupled subsystems. By the fact that the provided Laplacian matrix is symmetric, and the results are given in [31] and [32], the decoupled and reduced-order model of the closed-loop system can be derived as

$$\begin{cases} \dot{\tilde{\zeta}}_{cl_i}=A_{cl_i}\tilde{\zeta}_{cl_i}(t)+B_{dcl_i}\tilde{d}_i(t)+B_{fcl_i}\tilde{f}_i(t)\\ \tilde{r}_i(t)=C_{cl_i}\tilde{\zeta}_{cl_i}(t)+D_{dcl_i}\tilde{d}_i(t)+D_{fcl_i}\tilde{f}_i(t)\\ \tilde{z}_i(t)=H_{cl_i}\tilde{\zeta}_{cl_i}(t). \end{cases} \tag{11}$$

The acquired transformation matrices and the definition of the new variables are provided with detail in Appendix VI-A.

Theorem 1: Consider the decomposed dynamic equation of DERs (11), consensus problem (4) and performance objectives (10) can be guaranteed simultaneously, and there exist positive-definite symmetric matrices $\Lambda_{1i}, \Lambda_{2i}, \Lambda_{3i}, \Lambda_{4i}$, matrices $\sigma_1, \sigma_2, \hat{\sigma}_2, N_1, N_2$ and positive scalars $\gamma_1, \gamma_2, \gamma_3, \beta$, such that for $i = 1, \ldots, n-1$ the MOO problem (12) is solved for $k = 1, 2, 3, 4$.

$$\begin{aligned} &\min_{\Lambda_{ki},\sigma_1,\sigma_2,\hat{\sigma}_2,N_1,N_2}\ \alpha_1\gamma_1+\alpha_2\gamma_1+\alpha_3\gamma_1-\alpha_4\beta\\ &\textbf{subject to}\\ &\begin{bmatrix} Herm(\mathrm{X}_i)+\Gamma_{1i} & \Gamma_{21i} & \Sigma_i+\Gamma_{31i}D_d\\ * & -\Theta(\sigma+\sigma^T) & \Theta\Sigma_i\\ * & * & \lambda_i^2D_d^TD_d+\gamma_1^2I \end{bmatrix}<0,\\ &\begin{bmatrix} Herm(\mathrm{X}_i)+\Gamma_4 & \Gamma_{23i} & \Sigma_i\\ * & -\Theta(\sigma+\sigma^T) & \Theta\Sigma_i\\ * & * & -\gamma_2^2I \end{bmatrix}<0,\\ &\begin{bmatrix} Herm(\mathrm{X}_i)+\Gamma_{1i} & \Gamma_{22i} & \Omega_i+\Gamma_{31i}D_f\\ * & -\Theta(\sigma+\sigma^T) & \Theta\Omega_i\\ * & * & \beta^2I-\lambda_i^2D_f^TD_f \end{bmatrix}<0,\\ &\begin{bmatrix} Herm(\mathrm{X}_i)+\Gamma_4 & \Gamma_{24i} & \Omega_i\\ * & -\Theta(\sigma+\sigma^T) & \Theta\Omega_i\\ * & * & -\gamma_3^2I \end{bmatrix}<0,\\ &B_u^T\sigma_2=\hat{\sigma}_2B_u^T \end{aligned} \tag{12}$$

where $\alpha_1, \alpha_2, \alpha_3, \Theta$ are positive constants, and variables are $\Gamma_{1i} = \lambda_i^2\begin{bmatrix} C & 0\end{bmatrix}^T\begin{bmatrix} C & 0\end{bmatrix}, \Gamma_4 = \begin{bmatrix} 0 & I\end{bmatrix}^T\begin{bmatrix} 0 & I\end{bmatrix}, \Gamma_{3i} = \lambda_i^2\begin{bmatrix} C & 0\end{bmatrix}^T, \Gamma_{2ki} = \Lambda_{ki}+\Theta X_i-\sigma^T, \sigma = diag(\sigma_1, \sigma_2)$ and

$$X_i=\begin{bmatrix} -\lambda_iC^TN_2^T & -N_1^TB_u^T\\ 0 & M_1^TB_u^T \end{bmatrix},$$
$$\Sigma_i=\begin{bmatrix} \sigma_1^TB_d-\lambda_iN_2D_d\\ \sigma_2^TB_d \end{bmatrix},\quad \Omega_i=\begin{bmatrix} \sigma_1^TB_f-\lambda_iN_2D_f\\ \sigma_2^TB_f \end{bmatrix}$$

Based on these relations, the filter parameters are now specified by $K = (N_1^T\hat{\sigma}_2^{-1})^T$ and $T = (N_2^T\hat{\sigma}_1^{-1})^T$. Proof of the Theorem is annexed in Appendix VI-B.

B. ROBUST DISTRIBUTED FAULT-TOLERANT CONTROL OF VOLTAGE AND FREQUENCY OF MGs

In this part, a robust distributed fault detection and fault-tolerant control of voltage and frequency of MGs are introduced. The proposed protocol should be determined to meet disturbance rejection and fault-tolerance conditions. Furthermore, the fluctuations of the primary layer should be compensated. Thus, the output voltage magnitude and frequency of each DER unit should be synchronized to their nominal value. Besides, according to equation (3) and considering the faults and disturbances in the dynamics of DERs, one obtains

$$\begin{aligned} \dot{\zeta}_i(t)&=B_uu_i(t)+B_dd_i(t)+B_ff_i(t)\\ y_i(t)&=C\zeta_i(t)+D_dd_i(t)+D_ff_i(t) \end{aligned} \tag{13}$$

where $\zeta_i(t) = (V_{\rm odi}(t), \omega_i(t))^T$ denotes the state vector, $u_i(t) = (u_i^v, u_i^\omega)^T$ expresses the control input vector, $d_i(t) = (d_i^v, d_i^\omega)^T$ is an L_2-norm bounded signal that represents unmodeled dynamics of the ith DERs, including unknown disturbances and uncertainties and $f_i(t) = (f_i^v, f_i^\omega)^T$ represents faults signal, and the superscripts v and ω corresponds to voltage and frequency, respectively. In order to

combine the relative information, the voltage and frequency output functions are defined as

$$\begin{cases} z_i^v(t) = V_{\text{ref}} - V_{\text{odi}}(t) \\ z_i^\omega(t) = \omega_{\text{ref}} - \omega_i(t) \end{cases} \tag{14}$$

and output function vector is defined as $z_i = (z_1^v, \ldots, z_n^v, z_1^\omega, \ldots, z_n^\omega)^T$. To achieve the model reference consensus in voltage and frequency, the following FDI filter is considered.

$$\begin{cases} \dot{\hat{\xi}}_i(t) = B_u u_i(t) + T r_i(t) \\ u_i(t) = K \hat{\xi}_i(t) \\ r_i(t) = \xi_i(t) - \hat{\xi}_i(t) \end{cases} \tag{15}$$

where $\hat{\xi}_i(t)$ represents the observer states vector, $r_i(t)$ represents the residual signal, and matrices T and K denote the filter gains to be selected and specified subsequently. Moreover, $\xi_i(t) = \sum_{j\in N_i}(y_i(t) - y_j(t) + b_i(y_i - y_{\text{ref}}))$ generates the relative output information and $\hat{\xi}_i(t) = C.\sum_{j\in N_i}(\hat{\xi}_i(t) - \hat{\xi}_j(t) + b_i(\hat{\xi}_i - y_{\text{ref}}))$, which, $b_i > 0$ if the ith DERs has access to the reference signal and otherwise, it is zero. To reach into the closed-loop system of voltage and frequency equation, by concatenating (13) and (15), the closed-loop dynamics can be derived as

$$\begin{cases} \dot{\zeta}_{\text{cl}} = A_{\text{cl}}\zeta_{\text{cl}}(t) + B_{\text{dcl}}D(t) + B_{\text{fcl}}F(t) \\ R(t) = C_{\text{cl}}\zeta_{\text{cl}}(t) + D_{\text{dcl}}D(t) + D_{\text{fcl}}F(t) \\ Z(t) = \widehat{C}_{\text{cl}}\zeta_{\text{cl}}(t) \end{cases} \tag{16}$$

where the variable are as $\delta_i(t) = \zeta_i(t) - \zeta_{\text{ref}}(t)$, $\zeta_{\text{ref}}(t) = ((V_{\text{ref}}1_n)^T, (\omega_{\text{ref}}1_n)^T)^T$, $\hat{\delta}_i(t) = \hat{\zeta}_i(t) - \hat{\zeta}_{\text{ref}}(t)$, $\hat{\zeta}_i(t) = (\hat{V}_{\text{odi}}(t), \hat{\omega}_i(t))^T$, $\hat{\zeta}_{\text{ref}}(t) = ((\hat{V}_{\text{ref}}1_n)^T, (\hat{\omega}_{\text{ref}}1_n)^T)^T$, $e_i(t) = \delta_i(t) - \hat{\delta}_i(t)$, $e = [e_1^T, \ldots, e_n^T]^T$, $\zeta = [\zeta_1^T, \ldots, \zeta_n^T]^T$, $\hat{\zeta} = [\hat{\zeta}_1^T, \ldots, \hat{\zeta}_n^T]^T$, $D = [d_1^T, \ldots, d_n^T]^T$, $R = [r_1^T, \ldots, r_n^T]^T$, $Z = [z_1^T, \ldots, z_n^T]^T$ and consequently, $\zeta_{\text{cl}} = \begin{bmatrix} e^T & \delta^T \end{bmatrix}^T$

$$A_{\text{cl}} = \begin{bmatrix} -\tilde{\mathcal{L}} \otimes TC & 0 \\ -I \otimes B_u K & I \otimes B_u K \end{bmatrix},$$
$$B_{\text{dcl}} = \begin{bmatrix} I \otimes B_d - \tilde{\mathcal{L}} \otimes TD_d \\ I \otimes B_d \end{bmatrix}, \; C_{\text{cl}} = \begin{bmatrix} \tilde{\mathcal{L}} \otimes C & 0 \end{bmatrix},$$
$$B_{\text{fcl}} = \begin{bmatrix} I \otimes B_f - \tilde{\mathcal{L}} \otimes TD_f \\ I \otimes B_f \end{bmatrix}, \; \widehat{C}_{\text{cl}} = \begin{bmatrix} 0 & \tilde{\mathcal{L}}_c \otimes I \end{bmatrix} \tag{17}$$

By the fact that the new Laplacian matrix $\tilde{\mathcal{L}}$ is non-singular (since $\tilde{\mathcal{L}} = \mathcal{L} + \mathcal{B}$ and the leader is connected to at least one node of graph), motivated by [31] and [32], there is a $\bar{J} \in \Re^{(2n)\times(2n)}$ such that $\bar{J}^T\mathcal{L}_1\bar{J} = diag(\lambda_1, \ldots, \lambda_{2n})$. By some algebraic computations the decomposed system can be achieved similar to (11). Details of transformation are presented in Appendix.

Theorem 2: Consider voltage and frequency dynamic equations of DERs, using the controller which is presented in (15), simultaneously distributed leader-follower fault detection and fault tolerant control can be achieved, if for $i = 1, \ldots, n$ the MOO problem formulated in (12) with the appropriate dimension variables and matrices is satisfied. Due to the similarity with Theorem 1, the details and proof of the theorem have been omitted.

Remark 1: Note that, by selecting the control signals $(u_i^v, u_i^\omega, u_i^P, u_i^Q, u_i^{\overline{\text{SoC}}})$, the nominal control inputs $V_i^{\text{nom}}, \omega_i^{\text{nom}}$ used in the droop control procedure can then be computed by the following equations:

$$\begin{cases} V_i^{\text{nom}} = \int (u_i^v + u_i^Q)dt \\ \omega_i^{\text{nom}} = \int (u_i^\omega + u_i^P)dt & DER \in DG \\ \omega_i^{\text{nom}} = \int (u_i^\omega + u_i^P + u_i^{\overline{\text{SoC}}})dt & DER \in BESS \end{cases} \tag{18}$$

TABLE 1. Microgrid's parameters.

Description	DG 1, 2, 3	DG 4, 5	BESS 1, 2, 3
$\mathbf{V_{dc}}$	680 V	680 V	540 V
Communication Delay	3×10^{-3} s	3×10^{-3} s	3×10^{-3} s
$\mathbf{m_i^P}$	1.5×10^{-4}	1.2×10^{-4}	1.7×10^{-4}
$\mathbf{n_i^Q}$	1.8×10^{-3}	1.6×10^{-3}	2×10^{-3}
$\mathbf{k_i^{\overline{SoC}}}$	–	–	1
$\mathbf{K_{PV}}$	0.05	0.1	0.04
$\mathbf{K_{IV}}$	390	420	370
$\mathbf{K_{PC}}$	10.5	15	9.5
$\mathbf{K_{IC}}$	16000	20000	14000
C	–	–	11kWh
$GridFilter$	$R_f = 0.01\,\Omega, L_f = 1.35\,\text{mH}, C_f = 50\,\mu F$		
$OutputConnector$	$R_c = 0.03\,\Omega, L_c = 0.35\,\text{mH}$		

Line 1 & Line 2 & Line 4	Line 3 & Line 5
$0.23\,\Omega + j\,0.347\,\text{mH}$	$0.35\,\Omega + j\,1.847\,\text{mH}$
Load 1 & Load 2 & Load 3	**Load 4 & Load 5**
$26\,\text{kW} + 11.6\,\text{kvar}$	$21\,\text{kW} + 13\,\text{kvar}$

C. DISTRIBUTED FDI

For distributed FDI, based on generated residuals, the thresholds $\mathcal{J}_{th_i}(t)$ and the evaluation functions $\mathcal{J}_{r_i}(t)$ should be determined. Therefore, based on [33], the upper and lower threshold values are selected as $\mathcal{J}_{\text{th}_i}^u = \sup_{f_i=0, d_i\in D} r_i(t)$ and $\mathcal{J}_{\text{th}_i}^l = \inf_{f_i=0, d_i\in D} r_i(t)$, respectively. By considering $\mathcal{J}_{r_i} = r_i(t)$ and defining the decision logic as "if" $r_i(t) > \mathcal{J}_{\text{th}_i}^u$ (for $f_i \neq 0$) or $r_i(t) < \mathcal{J}_{\text{th}_i}^l$ (for $f_j \neq 0$, $j \in N_i$), "then" faulty unit can be detected. For isolation of the faults, the flags ρ_i, $i \in \mathcal{V}$ are defined and if $r_i(t) > \mathcal{J}_{\text{th}_i}^u$ or $r_i(t) < \mathcal{J}_{\text{th}_i}^l$, the $\rho_i = 1$ and 0 otherwise. Therefore, DERs share their flags with each other and make the pattern as $\mu_i = \{\rho_i, j \in N_i\}, i \in \mathcal{V}$. If all the elements of μ_i are equal to one, then the ith DER will be considered as a faulty unit.

Remark 2: In all systems using communication infrastructures, delays are inherent. Also, they have a significant deteriorating impact on MG's performance. It will cause synchronization problems, thereby downgrading the performance and even making the MG unstable. This matter necessitates characterizing the communication delays' effects on the MGs' stability while synthesizing a distributed control

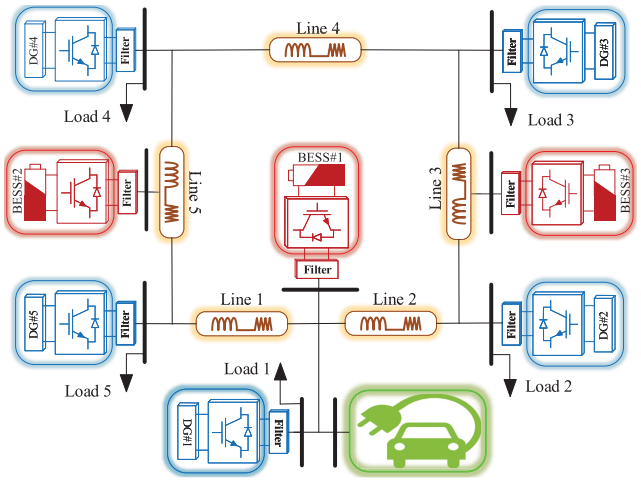

FIGURE 3. Single-line diagram of the test MG system.

scheme. Several researchers have investigated the various communication delays' impacts on MGs. Nevertheless, although communication delays have been considered in all of the provided simulations, this article has not theoretically contributed to delay-related issues specifically.

IV. SIMULATION RESULTS

The performance of the proposed control scheme is verified through various simulations in MATLAB/Simulink. The test system is an islanded, 480-V, 60-Hz MG demonstrated in Fig. 3. The parameters are given in Table 1. Two simulation scenarios are studied for different conditions. In the first scenario, the MG has five DGs and the effect of actuator faults and disturbances are investigated. In the second scenario, in addition to the DGs, BESSs and plug-in hybrid electric vehicles (PHEVs) fast-charging stations are considered. In this case, the proposed algorithm is studied in response to the sensor faults and disturbances in BESSs. Finally, a comparison is made with existing methods. Another point to consider is reactive power control; as stated in [34], due to the effects of transmission line impedance, accurate control of reactive power sharing and voltage regulation at the same time is not possible. Therefore, due to the importance of the voltage control in MGs, the main focus is on voltage regulation in this paper. Additionally, it is worthy of note that the faults considered in this research and provided results (simulations and experiments) are so general. As a result, one can regard them as data integrity attacks—among different categories of cyberattacks—impacting the MG's distributed control with unknown, limited bounds.

A. SCENARIO #1: MG WITH VOLTAGE-SOURCE CONVERTER BASED (VSC-BASED) DGs (WITH 3-ms COMMUNICATION DELAY)

In this section, the MG shown in Fig. 3 has been considered without BESSs and PHEVs, so the communication between DGs are according to $N_1 = \{2, 5\}, N_2 = \{1, 3\}, N_3 = \{2, 4\}, N_4 = \{3, 5\}, N_5 = \{4, 1\}$, and the disturbance matrix of DG units are considered as $B_d = [0.1 \;\; 0.2 \;\; 0.3 \;\; 0.4 \;\; 0.5]^T$, $D_d = [0.5 \;\; 0.4 \;\; 0.3 \;\; 0.2 \;\; 0.1]^T$, $D(t) = [1.7w(t) \;\; 1.5w(t) \;\; 1.1w(t) \;\; 1.3w(t) \;\; 1.8w(t)]^T$, where $w(t)$ is an energy limited white noise. A 3-ms communication delay has also been taken into account here. In the simulations, and without loss of generality, the actuator faults in the voltage of DGs has been considered, and the voltage actuator faults matrix of DGs has been selected as $B_f^v = [0 \;\; 0 \;\; 1 \;\; 1 \;\; 0]^T$. Further, by selecting positive constant weights $\alpha_1, \alpha_2, \alpha_3, \alpha_4$ equal to one (where give the equal rate of importance in the detection and control objectives) and $\Theta = 0.07$ the optimization problem is solved for voltage of DGs and parameter are derived as $\gamma_1 = 0.665, \gamma_2 = 0.346, \gamma_3 = 0.21e-3, \beta = 0.622$ and filter gains are $F = [3.021 \;\; 2.036 \;\; -2.025 \;\; -1.042 \;\; -0.069]^T$ and $T = [-4.068 \;\; -2.078 \;\; 2.045 \;\; 3.033 \;\; 4.031]^T$. Moreover, by considering the worst case analysis, the thresholds selected as $\mathcal{J}_{\text{th}_i}^l = [-0.15 \;\; -0.2 \;\; -0.2 \;\; -0.2 \;\; -0.2 \;\;]^T$ and $\mathcal{J}_{\text{th}_i}^u = [-0.2 \;\; -0.2 \;\; -0.2 \;\; -0.2 \;\; -0.2 \;\;]^T$ for voltage of DGs. Additional to mathematics FDI and tolerability analysis of the method, the following scenarios are considered to show the robustness of method.

1) At $t = 0$ s, simulation initialization period. Only the primary control is activated.
2) At $t = 1$ s, the proposed distributed FDI and control strategy are applied to the secondary layer.
3) The multiple abrupt actuator faults are simulated as a rectangular pulsed signal with an amplitude $f_3^v(t) = 2$ in the voltage of DG #3 during the time interval 3–3.5 s and amplitude $f_4^v(t) = 3$ in the voltage of #4 during the time interval 4.5–5 s.
4) At $t = 6$ s, the Load #2 is increased by 75%, then decreased to its default value at $t = 7$ s.
5) At $t = 8$ s, a line outage is occurred. Line#3 is disconnected from side DG#3 and reconnected at $t = 9$s.

At the beginning of the simulation, the MG is separated from the utility grid and operates in islanded operation mode. During first second of the process, the MG operates under the primary controller alone. As Fig. 4 displays, especially through the first second of operation, the MG voltage and frequency deviate from their nominal values. Consequently, the MG frequency and voltage must be recovered in secondary control layer. In order to validate the proposed distributed FDI and control strategy the effectiveness of the secondary control at $t = 1$ s is activated. As Fig. 4 shows, the distributed strategy can compensate for the droop-controller fluctuations, and fast restore both frequency and voltage to their nominal rates. Furthermore, active power-sharing is well established.

In order to investigate the effect of the designed control algorithm against the actuator faults, it is assumed that at periods 3–3.5 s and 4.5–5 s, the fault signal is applied to the voltage of DGs. As it can be seen, by applying the fault, the voltage deviates from its nominal value, and when the fault is terminated, the system quickly reaches its stable condition.

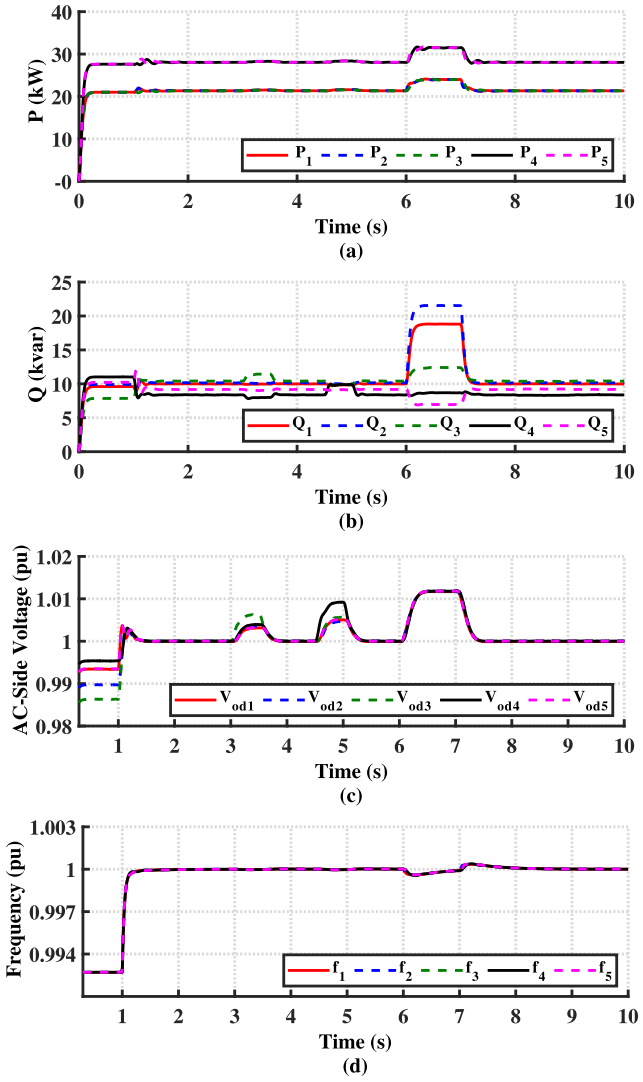

FIGURE 4. Performance evaluation of proposed scheme: (a) output active power of DGs, (b) output reactive power of DGs, (c) voltage regulation of DGs, and (d) frequency regulation of DGs.

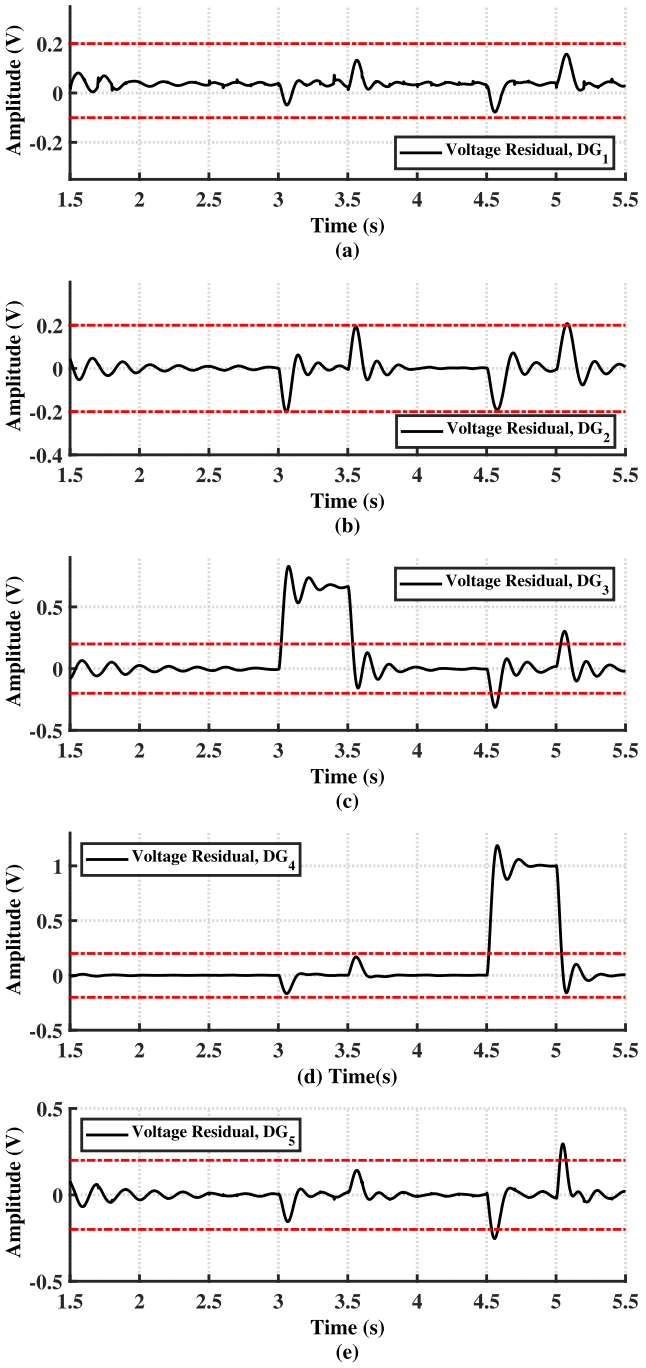

FIGURE 5. Generated residual signals during the time 1.5–5.5 s for: (a) voltage of DG #1, (b) voltage of DG #2, (c) voltage of DG #3, (d) voltage of DG #4, (e) voltage of DG #5. The dash-dot lines denote the residual upper and lower thresholds.

This case indicates the excellent performance of the designed control algorithm.

To highlight the proposed method performance toward load changes at $t = 6$ s, Load #2 abruptly increased by 75%. The results confirm that the distributed method can restore the MG frequency and voltages after a short transient time. At $t = 8$ s, when the switch in the Line #3 is opened, a slight deviation is occurred in the powers of DG #4, and the proposed method simply controlled it.

As demonstrated in Fig. 4, the voltage and frequency deviations are caused by the primary layer are compensated and also, active power-sharing of DGs is acceptable. Based on generated residual signals, it can be concluded that the proposed method is robust against disturbances and faults, and moreover fault sensitivities are enhanced and faults are well discriminated from the external disturbances. This method not only detects its own faults but also the faults of its nearest neighboring unit successfully. To demonstrate capabilities of fault isolation algorithm, the actuator fault in the voltage of DG #3 is considered. The residual signals are illustrated in Fig. 5, fault patterns $\mu_i, i = 1, 2, 3, 4, 5$, are obtained as $\mu_1 = \{0, 1, 0\}$, $\mu_2 = \{1, 0, 1\}$, $\mu_3 = \{1, 1, 1\}$, $\mu_4 = \{1, 1, 0\}$, $\mu_5 = \{0, 1, 0\}$. It is obvious that all elements of μ_3 are equal to one, and therefore the DG #3 is faulty.

B. SCENARIO #2: MG INCLUDING VSC-BASED DGs, BESSs, AND PHEV RAPID CHARGING STATION (WITH 3-ms COMMUNICATION DELAY)

This part aims to attain a desirable SOC balance of BESSs and voltage and frequency coordination and realize active power-sharing; a 3-ms communication delay has also been considered in this subsection. The initial charge of BESSs is randomly chosen. Note that the nominal capacity of the energy storage units is selected as 20.3 kWh. Nevertheless, due to the simulation studies inadequate time, the storage units capacity is assumed to be 0.4% of their nominal value. Contrarily, the variation in SOCs would be insignificant through the simulation time.

The disturbance matrix and communication between DGs are considered as IV-A and communication between BESSs are defined as $N_1 = \{2, 3\}, N_2 = \{1, 3\}, N_3 = \{2, 1\}$ accordingly the disturbance matrix of BESSs are as; $B_d = [0.15 \quad 0.25 \quad 0.35]^T$, $D_d = [0.55 \quad 0.45 \quad 0.35]^T$, $D(t) = [1.75w(t) \quad 1.55w(t) \quad 1.15w(t)]^T$, where $w(t)$ is an energy limited white noise. Here, we investigate the impact of sensor faults on BESSs; therefore, we consider sensor fault signal with an amplitude $f_3^{\omega}(t) = 2.5$ in the frequency of BESS #2 during the time interval 3–3.5 s occur. Accordingly, frequency sensor faults matrix of the BESSs is selected as $D_f^{\omega} = [0 \quad 1 \quad 0]^T$. Besides, by selecting positive constant weights $\alpha_1, \alpha_2, \alpha_3, \alpha_4$ equal to one, and $\Theta = 0.32$ the optimization problem is solved for DGs and parameter are derived as $\gamma_1 = 0.325, \gamma_2 = 1.036, \gamma_3 = 0.18 \times 10^{-3}, \beta = 1.737$ and filter gains are $F[4.13 \quad 2.701 \quad -1.009 \quad -2.73 \quad -1.121]^T$ and $T = [-2.801 \quad -1.662 \quad 3.033 \quad 4.187 \quad 2.602]^T$, and resolved again for BESSs and parameters are derived $\gamma_1 = 0.71, \gamma_2 = 0.33, \gamma_3 = 0.7 \times 10^{-3}, \beta = 4.01$ and filter gains are $F = [1.333 \quad 3.412 \quad -1.786]^T$ and $T = [-1.008 \quad -3.036 \quad 2.78]^T$, respectively. Toward this end, the subsequent test scenarios are carried:

1) At $t = 0$ s, the primary control is activated.
2) At $t = 1$ s, the proposed distributed FDI and control strategy are applied to the secondary layer of both DGs and BESSs.
3) The multiple abrupt sensor faults are simulated as a rectangular pulsed signal with an amplitude $f_2^{\omega}(t) = 2.5$ in the frequency of BESS #2 during the time interval 3–3.5 s.
4) At $t = 4.5$ s, the Load #2 is increased by 75%, then decreased to its default value at $t = 5.5$ s.
5) At $t = 6.5$ s, the DG #4 is plugged out from the MG and plugged in at $t = 10$ s.
6) At $t = 7$ s, a line outage is occurs. Line#3 is disconnected from side DG#3 and reconnected at $t = 8$ s.
7) In the period 9–11 s, the charge mode of the PHEV [35] is checked. The PHEV with the initial charge of 30% is connected to the MG through Bus #1 shown in Fig. 3 and then disconnected at $t = 11$ s.

As can be seen from the simulation results in Fig. 6, 7, 8 and 9, and the same as the previous scenario, the voltage, frequency, and active power are well controlled, and also the SOC of BESSs are in balance. The designed control algorithm also has a robust performance against sensor fault. Besides, it is fully adaptable to the plug and play (PnP) capabilities as well as the PHEV charging and has a stable performance.

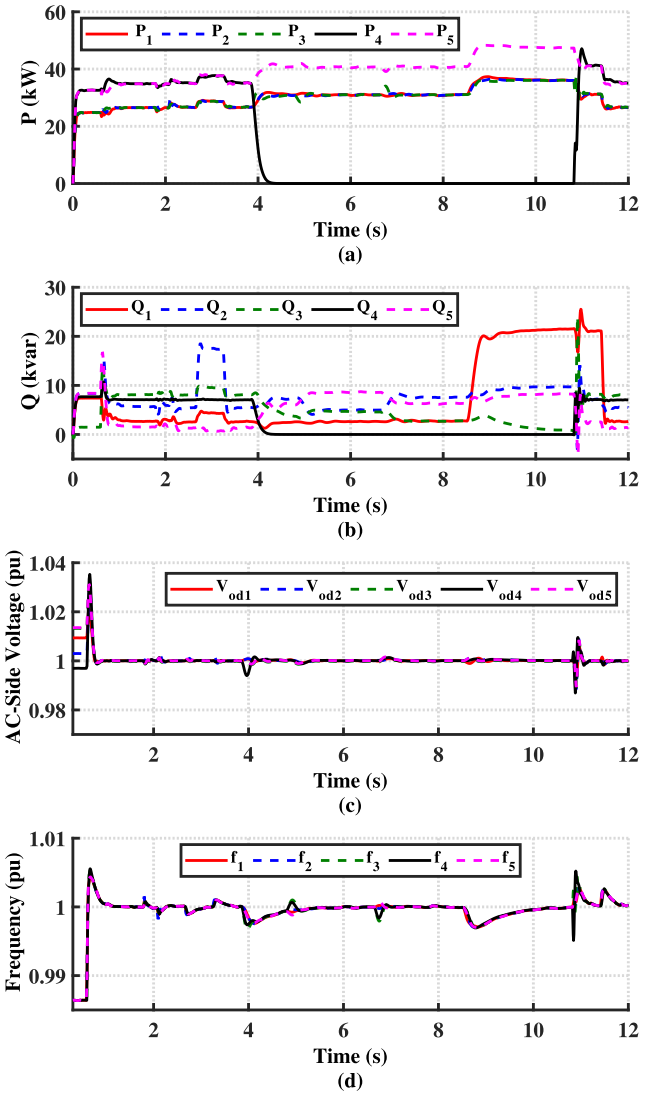

FIGURE 6. Performance evaluation of proposed scheme: (a) output active power of DGs, (b) output reactive power of DGs, (c) voltage regulation of DGs, and (d) frequency regulation of DGs.

C. COMPARISON WITH SIMILAR RESEARCH STUDIES

Finally, to show the superiority of the proposed control strategy over other methods, we compare it with other previously-reported techniques. Associated with the previously methods provided for the faults tolerant, the method specified in this paper has many features. Compared to the methods used by the common Lyapunov function to solve the fault problem, there is much more freedom of action due to the use of four functions to the optimization of the problem. In this method, by selecting different control weights $(\rho_1, \rho_2, \rho_3, \rho_4)$,

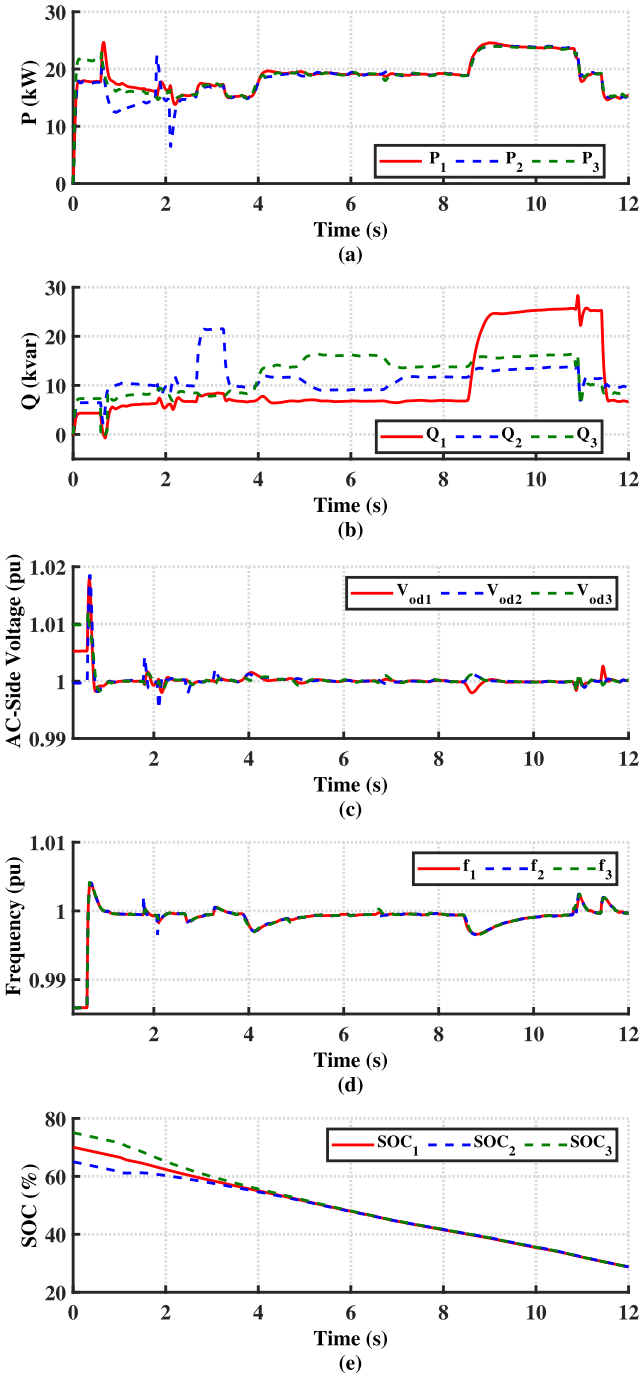

FIGURE 7. Performance evaluation of proposed scheme: (a) output active power of BESSs, (b) output reactive power of BESSs, (c) voltage regulation of BESSs, (d) frequency regulation of BESSs, and (e) SOC balance of BESSs.

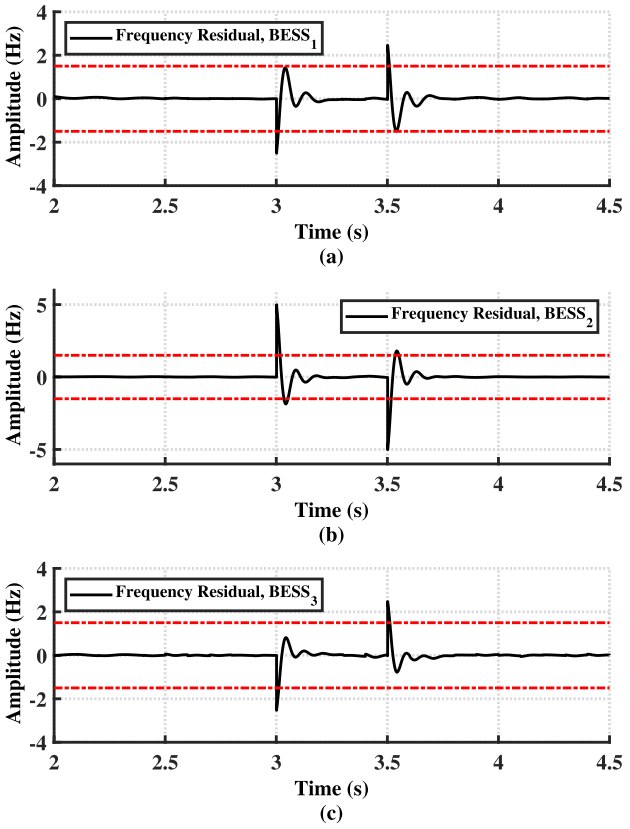

FIGURE 8. Generated residual signals during the time 2–4.5 s for: (a) frequency of BESS #1, (b) frequency of BESS #2, (c) frequency of BESS #3.

a trade-off between the objective function can be designed as desired, which reduces conservatism.

Further, the proposed method can be solved by centralized methods. In this case, if the number of agents N increases, implementation of equation (10) will be very challenging. In this method, the system order was reduced using ''model transformation'' and converted to N separate subsystems. Motivated by [32] can be shown that the order of the computational complexity is also reduced by a factor of $N^2/(N-1)$ for the Theorem 1 and by a factor N for Theorem 2. Unlike the methods presented in [24], [25], [28], [36] and [33], which used separate algorithms for generating control signal in parallel, in this study, both state estimator and proposed control algorithm have been integrated to solve the problem for each agent. This potentially reduces the computational complexity of the problem.

In addition to theoretical comparisons, in order to show the proposed method's effectiveness, the results will be compared with the technique presented in [37], which controls the voltage and frequency in the secondary layer by performing simulations for the actuator fault in an MG including DG. At $t = 3$ s, the actuator faults are considered in voltage and frequency measurements of DG #2, where $f_2^v(t) = 3\sin(7t)$, $f_2^f(t) = 1\sin(2t)$. The simulation results are shown in Fig. 10. Because the method proposed in [37] does not has safety upon actuator faults, the voltage and frequency waveforms start oscillating when the actuator faults happen. In contrast, the proposed method's ability to satisfy the necessity of the fault effects operation is verified.

V. EXPERIMENTAL RESULTS

In order to examine the proposed controller's effectiveness, three VSCs are required at least. Based on the facilities available at Georgia Southern University, three VSCs (one

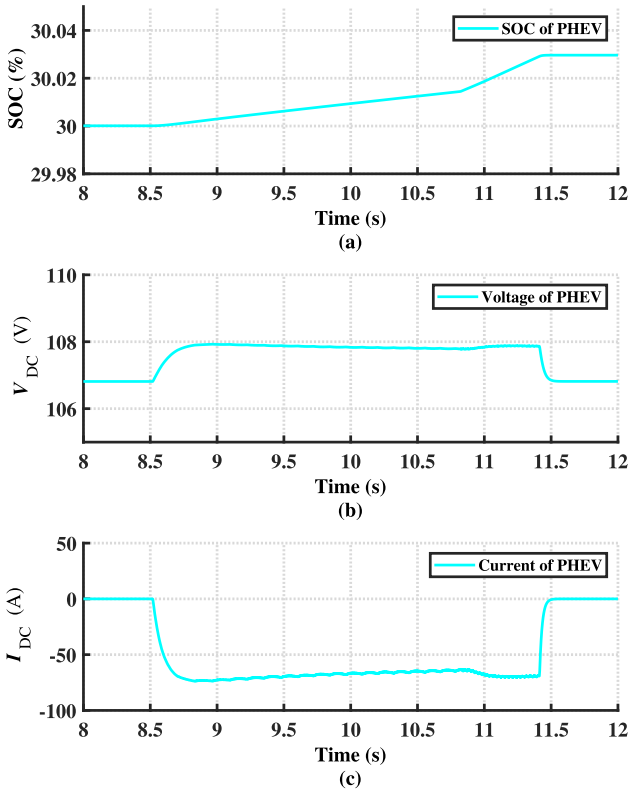

FIGURE 9. Performance evaluation of proposed scheme: (a) SOC of PHEV, (b) voltage of PHEV, and (c) current of PHEV.

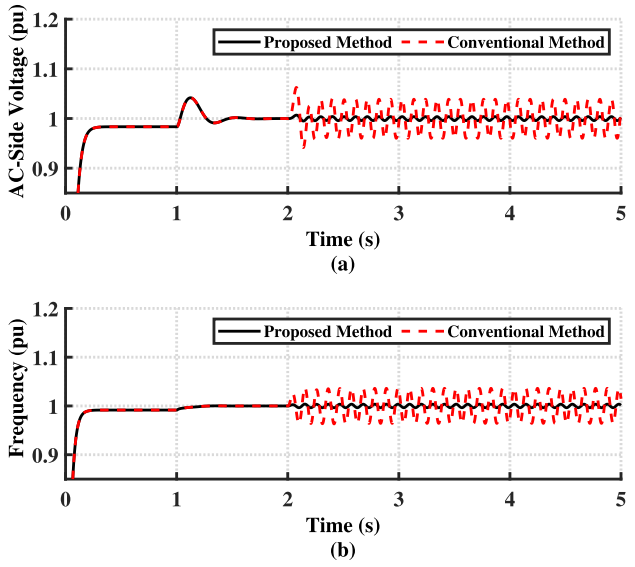

FIGURE 10. Comparison of the proposed method with previously-reported techniques in [37]: (a) voltage of DG #2, (b) frequency of DG #2.

of which has been depicted in Fig. 11 in detail) have been employed to conduct experimental examinations. The parameters of one of them have been reported in Table 2. The VSC uses SEMIKRON intelligent power modules based on insulated gate bipolar transistors (IGBTs) (i.e., "SKM 50 GB 123 D" modules). Additionally, SEMIKRON "SKHI

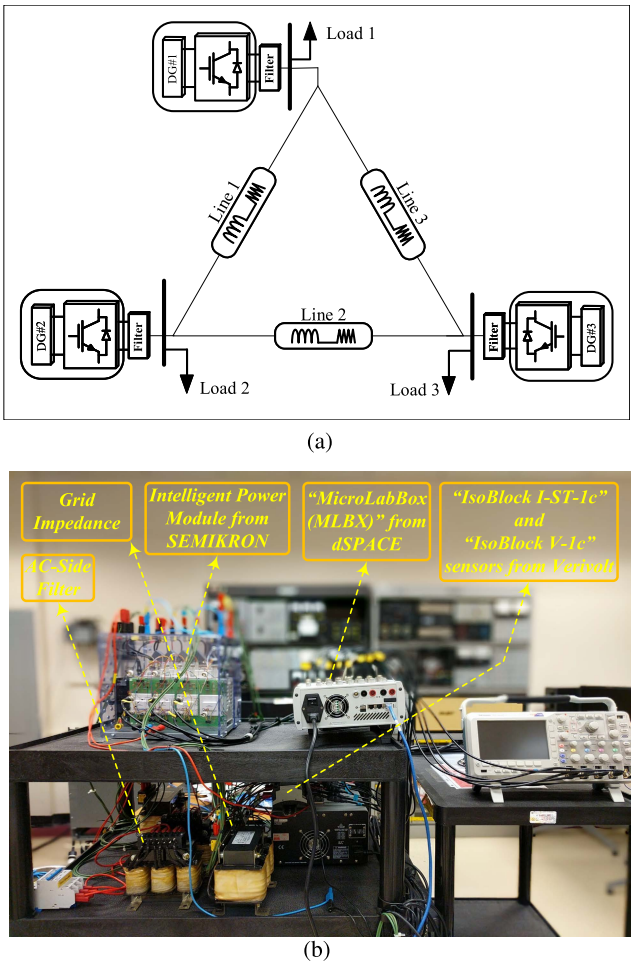

FIGURE 11. Experimental test rig: (a) arrangement of VSCs (b) one of the VSC setups used in the test rig for conducting experiments.

TABLE 2. Parameters of Fig. 11.

Parameter	Value	Parameter	Value
S_n [1]	10.81 kVA	f_s [2]	8.1 kHz
L_{f1}/R_{f1}	1.1 mH/0.01 Ω	$V_{\text{PCC}_{\text{Line-to-Line rms}}}$ [1]	208 V
L_{f2}/R_{f2}	1.1 mH/0.01 Ω	V_{DC} [1]	400 V
C_f/R_f	15.40 μF/2.08 Ω		

[1] Nominal Value [2] Switching Frequency

21A (R)" gate drives and protection circuitry are used in order to operate the VSC. Verivolt "IsoBlock I-ST-1c"/"IsoBlock V-1c" current/voltage sensors have been hooked to digital inputs; they are utilized in order to measure the currents and the voltages, respectively. dSPACE "MicroLabBox (MLBX)" using field-programmable gate arrays (also known as FPGAs) and real-time processor connects the VSCs under test to the printed circuit boards of the drive and measurement circuits; it also generated PWM signals via relevant digital inputs/outputs.

Based on the test setup available at Georgia Southern University, three scenarios could be considered in order to verify the practicality of the proposed algorithm. To this end, the

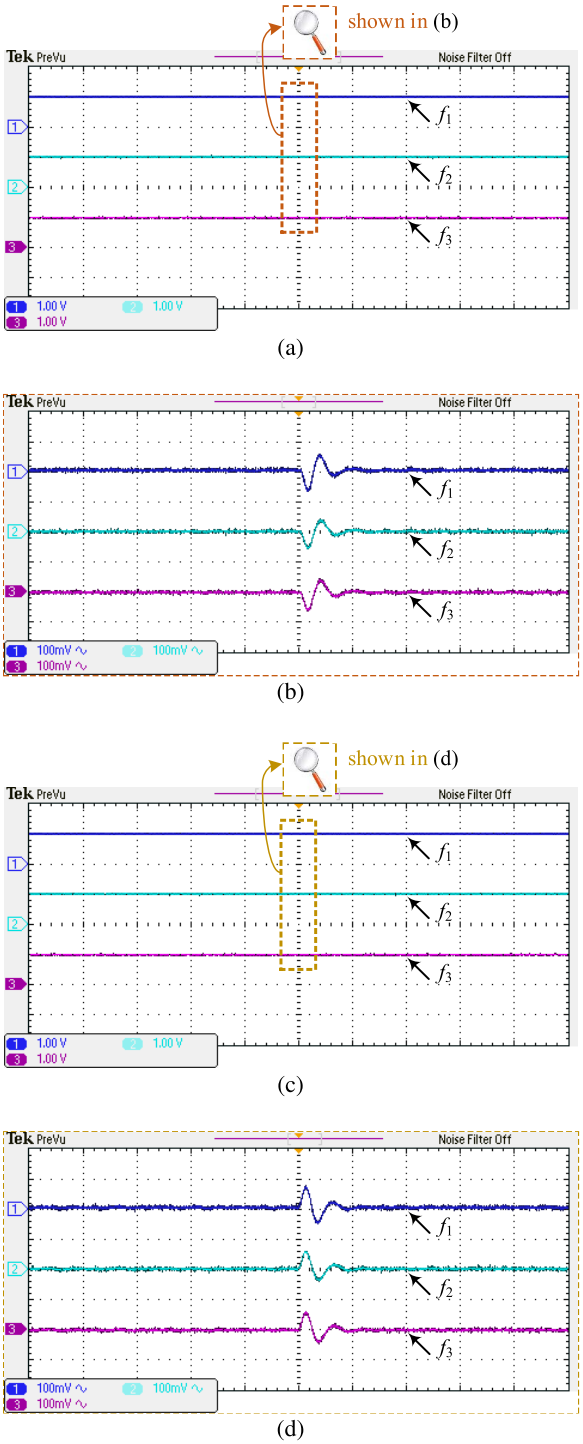

FIGURE 12. Experimental results associated with the frequency regulation: (a) frequency for the load connection test with the traces in blue, cyan, and magenta, for VSC #1, #2, and #3, respectively, with 60 Hz/div (their "actual" per-unit (pu) values have been noted at the left-bottom corner of the figure); (b) the ac components of the frequency signals depicted in Fig. 12a with 0.06 Hz/div (the "percentage" pu values have been indicated at the left-bottom corner of the figure) (c) frequency for the load disconnection test with the signal information detailed in Fig. 12a; (d) the ac components of the frequency signals depicted in Fig. 12c with the signal information detailed in Fig. 12b all with 1.00 s/div.

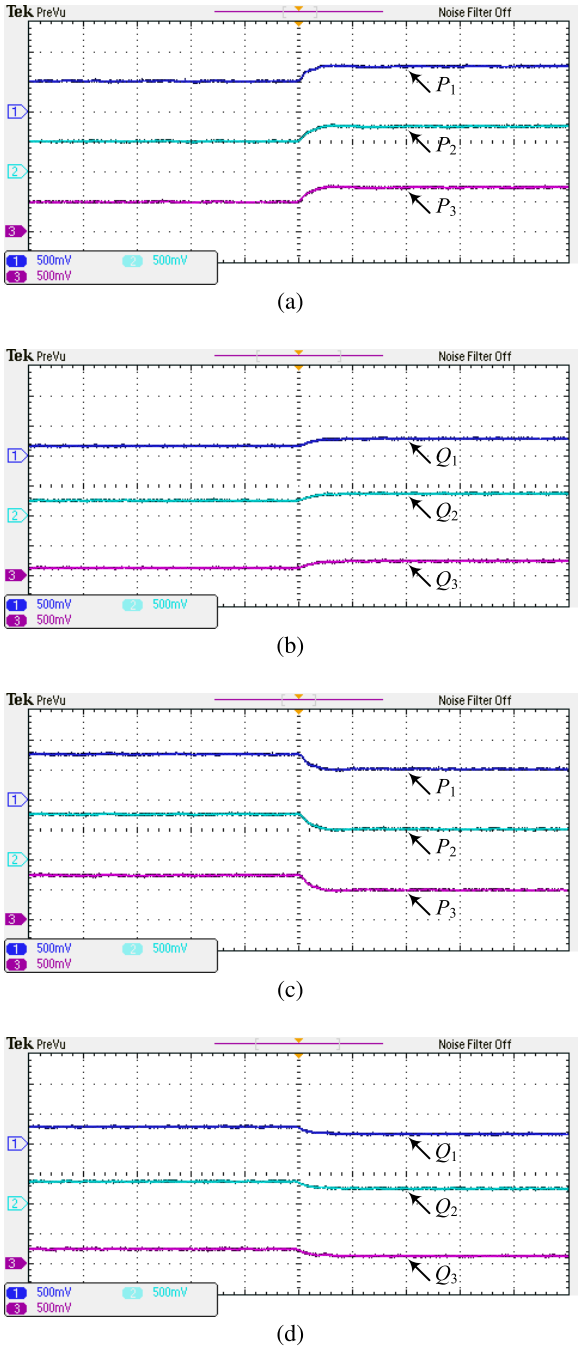

FIGURE 13. Experimental results associated with the active/reactive power variations: (a) active power for the load connection test with the traces in blue, cyan, and magenta, for VSC #1, #2, and #3, respectively, with 5.40 kW/div; (b) reactive power for the load connection test with the traces in blue, cyan, and magenta, for VSC #1, #2, and #3, respectively, with 5.40 kvar/div (c) active power for the load disconnection test with the traces in blue, cyan, and magenta, for VSC #1, #2, and #3, respectively, with 5.40 kW/div; (d) reactive power for the load disconnection test with the traces in blue, cyan, and magenta, for VSC #1, #2, and #3, respectively, with 5.40 kvar/div (all of the "actual" pu values have been noted at the left-bottom corner of the figure) all with 0.5 s/div.

impacts of load connection, load disconnection, and voltage sensor fault are investigated in three separate scenarios on our test setup. Disturbance matrix and communication between DGs are considered similar to Scenario #2 for BESSs, and voltage sensor fault signal with an amplitude $f_1^v(t) = 2.5$ in the voltage of DG #1 occur.

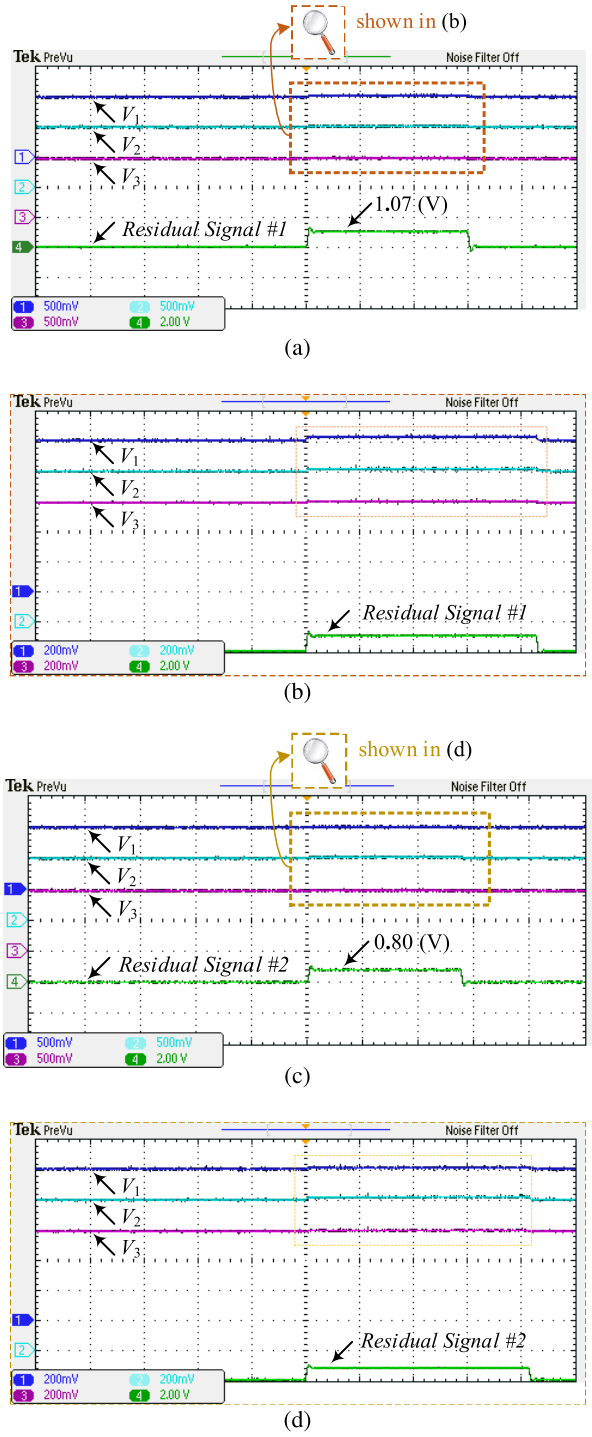

FIGURE 14. Experimental results associated with the ac-side voltage and sensor faults (fault signals): (a) ac-side voltage with the traces in blue, cyan, and magenta, for VSC #1, #2, and #3, with 104 V/div (line-to-line rms) and the residual signal with 2 V/div, respectively, for the fault signal applied to VSC #1; (b) the enlarged view of the signals in Fig. 14a with 41.6 V/div (line-to-line rms) (c) ac-side voltage with the traces in blue, cyan, and magenta, for VSC #1, #2, and #3, with 104 V/div (line-to-line rms) and the residual signal with 2 V/div, respectively for the fault signal applied to VSC #2; (d) the enlarged view of signals in Fig. 14c with 41.6 V/div (line-to-line rms) (all of the "actual" pu values have been noted at the left-bottom corner of the figures) all with 0.5 s/div.

Figs. 12–14 have depicted the experimental outcomes from the proposed method. It is noteworthy that in the experiments, the frequency signals' ac components are required to show the frequency variations as included in Figs. 12b and d. Also, it is worthy of mention that Figs. 14a and b could have only shown VSC #1'sensor fault while Figs. 14c and d could have solely presented VSC #2'sensor fault. The agreement demonstrated in simulations and experimental results, which are consistent all together, reveals the efficacy of the proposed fault-tolerant distributed control.

VI. CONCLUSION

In this paper, an innovative, fault-tolerant, distributed control scheme—including robust, distributed, simultaneous, passive FDI—has been proposed for islanded ac MGs based on relative output information. By the proposed algorithm, voltage, frequency, and active power-sharing among DERs and an SOC balance between BESSs have been accomplished, considering sensor and actuator faults. The way that the faults are modeled and seen in this article is so that they are able to include cyberattacks/cyber threats (mostly in the form of data integrity attacks), sensor-related issues, and so on, and the considered faults' nature has been general. The theoretical concepts, including a mathematical model of the MG, theorems, and design procedure of the proposed method based on H_∞/H_- optimization have been presented. The performance of the controller has been evaluated for sensor and actuator faults, as well as small- and large-signal disturbances, in the MATLAB/Simulink environment. It has also been compared with the performance of other commonly used distributed control strategies. Finally, the proposed methodology's effectiveness has been verified via experimental results.

APPENDIX

A. DETAILS OF THE REDUCED ORDER TRANSFORMATION AND DECOMPOSED MODEL

To reduce the order of (8), by defining variables $\bar{e}(t) = (\mathcal{L}_c \otimes I_n)e(t)$ and $\bar{\zeta}(t) = (\mathcal{L}_c \otimes I_n)\zeta(t)$, and considering Lemma 2 in [30], there exist an orthogonal matrix $U = \begin{bmatrix} U_1 & U_2 \end{bmatrix}$ with $U_2 = 1_n/\sqrt{n}$ such that, $U^T\mathcal{L}_c U = diag(I_{n-1}, 0)$, $U^T\mathcal{L}U = diag(\mathcal{L}_1, 0)$ is positive-definite matrix for connected graph. By utilizing this transformation $\widehat{e} = (U^T \otimes I_n)\bar{e}, \widehat{\zeta} = (U^T \otimes I_n)\bar{\zeta}, \widehat{R} = (U^T \otimes I_n)R, \widehat{\mathbf{Z}} = (U^T \otimes I_n)\mathbf{Z}, \widehat{D} = (U^T \otimes I_n)D, \widehat{F} = (U^T \otimes I_n)F$ and some calculations, the following reduced order model can be derived:

$$\begin{cases} \dot{\hat{\zeta}}_{\rm cl}(t) = \begin{bmatrix} \hat{A}_1 & 0 \\ \hat{A}_2 & \hat{A}_3 \end{bmatrix} \hat{\zeta}_{\rm cl}(t) + \begin{bmatrix} \hat{B}_1 \\ \hat{B}_2 \end{bmatrix} \hat{D}(t) + \begin{bmatrix} \hat{B}_3 \\ \hat{B}_4 \end{bmatrix} \hat{F}(t) \\ \hat{R}(t) = \begin{bmatrix} \hat{C}_1 & 0 \end{bmatrix} \hat{\zeta}_{\rm cl}(t) + \mathcal{L}_1 \otimes D_d\hat{D}(t) + \mathcal{L}_1 \otimes D_f\hat{F}(t) \\ \hat{Z} = \begin{bmatrix} 0 & I_{n-1} \otimes I_3 \end{bmatrix} \hat{\zeta}_{\rm cl}(t) \end{cases} \tag{19}$$

where, $\hat{\zeta} = [\widehat{\zeta}_1^T, \ldots, \widehat{\zeta}_{n-1}^T]^T, \hat{e} = [\widehat{e}_1^T, \ldots, \widehat{e}_{n-1}^T]^T, \hat{\xi}_{\text{cl}} = \left[\hat{e}^T \ \hat{\zeta}^T\right]^T, \hat{Z} = [\widehat{Z}_1^T, \ldots, \widehat{Z}_{n-1}^T]^T, \hat{F} = [\widehat{f}_1^T, \ldots, \widehat{f}_{n-1}^T]^T, \hat{D} = [\widehat{D}_1^T, \ldots, \widehat{D}_{n-1}^T]^T, \hat{R} = [\widehat{R}_1^T, \ldots, \widehat{R}_{n-1}^T]^T, \hat{A}_1 = (-L_1 \otimes TC), \hat{A}_2 = -I_{n-1} \otimes B_u K, \hat{A}_3 = I_{n-1} \otimes B_u K, \hat{B}_1 = I_{n-1} \otimes B_d - L_1 \otimes TD_d, \hat{B}_2 = I_{n-1} \otimes B_d, \hat{B}_3 = I_{n-1} \otimes B_f - L_1 \otimes TD_f, \hat{B}_4 = I_{n-1} \otimes B_f, \hat{C}_1 = L_1 \otimes C$. It is clear that, based on this relationships $\|T_{ZD}\|_\infty = \left\|T_{\hat{Z}\hat{D}}\right\|_\infty, \|T_{RD}\|_\infty = \left\|T_{\hat{R}\hat{D}}\right\|_\infty, \|T_{ZF}\|_\infty = \left\|T_{\hat{Z}\hat{F}}\right\|_\infty, \|T_{RF}\|_-^+ = \left\|T_{\hat{R}\hat{F}}\right\|_-$.

In order to decompose the equation (19) into the first order subsystems, based on provided results in [31] and [32], there is an orthogonal matrix $J \in \Re^{(n-1)\times(n-1)}$ such that $J^T \mathcal{L}_1 J = diag(\lambda_1, \ldots, \lambda_{n-1})$. By reformulating the variable as $\left[\tilde{\zeta}_1^T, \ldots, \tilde{\zeta}_{n-1}^T\right]^T = (J^T \otimes I_3)\hat{\zeta}, \left[\tilde{e}_1^T, \ldots, \tilde{e}_{n-1}^T\right]^T = (J^T \otimes I_3)\hat{e}, \left[\tilde{d}_1^T, \ldots, \tilde{d}_{n-1}^T\right]^T = (J^T \otimes I_3)\hat{d}, \left[\tilde{f}_1^T, \ldots, \tilde{f}_{n-1}^T\right]^T = (J^T \otimes I_3)\hat{F}, \left[\tilde{Z}_1^T, \ldots, \tilde{Z}_{n-1}^T\right]^T = (J^T \otimes I_3)\hat{Z}, [\tilde{r}_1^T, \ldots, \tilde{r}_{n-1}^T]^T = (J^T \otimes I_3)\hat{R}$ consequently,

$$\begin{cases} \dot{\tilde{\xi}}_{cl_i} = A_{cl_i}\tilde{\xi}_{cl_i}(t) + B_{dcl_i}\tilde{d}_i(t) + B_{fcl_i}\tilde{f}_i(t) \\ \tilde{r}_i(t) = C_{cl_i}\tilde{\xi}_{cl_i}(t) + D_{dcl_i}\tilde{d}_i(t) + D_{fcl_i}\tilde{f}_i(t) \\ \tilde{z}_i(t) = H_{cl_i}\tilde{\xi}_{cl_i}(t) \end{cases} \tag{20}$$

where, $A_{cl_i} = \begin{bmatrix} -\lambda_i TC & 0 \\ -B_u K & B_u K \end{bmatrix}, \tilde{\zeta}_{cl_i} = \begin{bmatrix} \tilde{e}_i(t) \\ \tilde{\zeta}_i(t) \end{bmatrix}, B_{dcl_i} = \begin{bmatrix} B_d - \lambda_i TD_d \\ B_d \end{bmatrix}, B_{fcl_i} = \begin{bmatrix} B_f - \lambda_i TD_f \\ B_f \end{bmatrix}, C_{cl_i} = \begin{bmatrix} \lambda_i C & 0 \end{bmatrix}, D_{dcl_i} = \lambda_i D_d, D_{fcl_i} = \lambda_i D_f, H_{cl_i} = \begin{bmatrix} 0 & I_{n-1} \end{bmatrix}$.

The above concludes the proof.

B. PROOF OF THEOREM 3.1

At first, the performance $\|T_{RD}\|_\infty = \left\|T_{\tilde{r}_i\tilde{d}_i}\right\|_\infty < \gamma_1$ is considered. The positive-definite Lyapunov function candidate $V_i(t) = \tilde{\zeta}_{cl_i}^T(t)\Lambda_{1i}\tilde{\zeta}_{cl_i}(t)$ is selected, where along of guarantee stability the time derivative of it must be as $\dot{V}_i(t) < \tilde{r}_i^T(t)\tilde{r}_i(t) + \gamma_1^2\tilde{d}_1^T(t)\tilde{d}_i(t)$. Based on (11), we can write:

$$\begin{bmatrix} I & 0 \\ A_{cl_i} & B_{dcl_i} \end{bmatrix}^T \begin{bmatrix} 0 & \Lambda_{1i} \\ \Lambda_{1i} & 0 \end{bmatrix} \begin{bmatrix} I & 0 \\ A_{cl_i} & B_{dcl_i} \end{bmatrix} + \begin{bmatrix} 0 & I \\ C_{cl_i} & D_{dcl_i} \end{bmatrix}^T \begin{bmatrix} \gamma_1^2 I & 0 \\ 0 & I \end{bmatrix} \begin{bmatrix} 0 & I \\ C_{cl_i} & D_{dcl_i} \end{bmatrix} < 0 \tag{21}$$

This inequality, can be reformulated as $M_U^T Z M_U < 0 < 0$,

$$Z = \begin{bmatrix} C_{cl_i}^T & \Lambda_{1i} & C_{cl_i}^T D_{dcl_i} \\ * & 0 & 0 \\ * & * & \Upsilon_{1i} \end{bmatrix}, \quad M_U = \begin{bmatrix} I & 0 \\ A_{cl_i} & B_{cl_i} \\ 0 & I \end{bmatrix} \tag{22}$$

where $\Upsilon_{1i} = D_{dcl_i}^T D_{dcl_i} - \gamma_1^2 I$. By defining the matrices M_V and V as

$$M_V = \begin{bmatrix} \Theta I & -I & 0 \\ 0 & 0 & I \end{bmatrix}^T, \quad V = \begin{bmatrix} I & \Theta I & 0 \end{bmatrix}$$

and by exerting the Projection lemma in [38], the inequality $M_U^T Z M_U < 0$ is equivalent to:

$$Z + Herm(\left[A_{cl_i} \ -I \ B_{dcl_i}\right]^T \left[\sigma \ \Theta\sigma \ 0\right]) < 0 \tag{23}$$

By using equations (22) and (23), and division σ into $\sigma = diag(\sigma_1, \sigma_2)$ the following inequality is obtained:

$$\begin{bmatrix} Herm(\Omega_1) + \Gamma_{1i} & \Lambda_{1i} + \Theta\Omega_1 - \sigma^T & \Omega_2 + \Gamma_{3i}D_d \\ * & -\Theta(\sigma + \sigma^T) & \Theta\Omega_2 \\ * & * & \lambda_i^2 D_d^T D_d - \gamma_1^2 I \end{bmatrix} < 0 \tag{24}$$

where $\Omega_1 = \begin{bmatrix} -\lambda_i C^T F^T \sigma_1 & -K^T B_u^T \sigma_2 \\ 0 & K^T B_u^T \sigma_2 \end{bmatrix}, \Omega_2 = \begin{bmatrix} \sigma_1^T B_d - \lambda_i \sigma_1^T F D_d \\ \sigma_2^T B_d \end{bmatrix}$. As can be seen, inequality (24) is not in the form of an LMI, therefore we employ the equality constraint $B_u^T \sigma_2 = \hat{\sigma}_2 B_u^T$ and by using the replacement $N_1^T = K^T \hat{\sigma}_2$, $N_2^T = F^T \sigma_1$ the first inequality in 12 is obtained. The proof of the other performance index by employing the same techniques can be reached easily. Therefore, these details are omitted to avoid over-explanation. The above ends the proof.

REFERENCES

[1] J. Rocabert, A. Luna, F. Blaabjerg, and P. Rodriguez, "Control of power converters in AC microgrids," *IEEE Trans. Power Electron.*, vol. 27, no. 11, pp. 4734–4749, Nov. 2012.
[2] J. M. Guerrero, J. C. Vasquez, J. Matas, L. G. de Vicuna, and M. Castilla, "Hierarchical control of droop-controlled AC and DC microgrids—A general approach toward standardization," *IEEE Trans. Ind. Electron.*, vol. 58, no. 1, pp. 158–172, Jan. 2011.
[3] M. Davari, M. P. Aghababa, F. Blaabjerg, and M. Saif, "An innovative, adaptive faulty signal rectifier along with a switching controller for reliable primary control of GC-VSIs in CPS-based modernized microgrids," *IEEE Trans. Power Electron.*, vol. 36, no. 7, pp. 8370–8387, Jul. 2021.
[4] M. Davari, H. Nafisi, M.-A. Nasr, and F. Blaabjerg, "A novel IGDT-based method to find the most susceptible points of cyberattack impacting operating costs of VSC-based microgrids," *IEEE J. Emerg. Sel. Topics Power Electron.*, vol. 9, no. 3, pp. 3695–3714, Jun. 2021.
[5] M. Davari, W. Gao, Z.-P. Jiang, and F. L. Lewis, "An optimal primary frequency control based on adaptive dynamic programming for islanded modernized microgrids," *IEEE Trans. Autom. Sci. Eng.*, vol. 18, no. 3, pp. 1109–1121, Jul. 2021.
[6] C. -T. Lee, C. -C. Chu, and P. -T. Cheng, "A new droop control method for the autonomous operation of distributed energy resource interface converters," *IEEE Trans. Power Electron.*, vol. 28, no. 4, pp. 1980–1993, Apr. 2013.
[7] M. Raeispour, H. Atrianfar, H. R. Baghaee, and G. B. Gharehpetian, "Robust hierarchical control of vsc-based off-grid AC microgrids to enhancing stability and FRT capability considering time-varying delays," *IEEE J. Emerg. Sel. Topics Power Electron.*, vol. 9, no. 6, pp. 7159–7172, Dec. 2021.
[8] M. Raeispour, H. Atrianfar, H. R. Baghaee, and G. B. Gharehpetian, "Robust sliding mode and mixed H_2/H_∞ output feedback primary control of AC microgrids," *IEEE Syst. J.*, vol. 15, no. 2, pp. 2420–2431, Jun. 2021.
[9] A. Parisio, E. Rikos, and L. Glielmo, "A model predictive control approach to microgrid operation optimization," *IEEE Trans. Control Syst. Technol.*, vol. 22, no. 5, pp. 1813–1827, Sep. 2014.
[10] H. R. Baghaee, M. Mirsalim, G. B. Gharehpetian, and H. A. Talebi, "A decentralized power management and sliding mode control strategy for hybrid AC/DC microgrids including renewable energy resources," *IEEE Trans. Ind. Informat.*, early access, Mar. 3, 2017, doi: 10.1109/TII.2017.2677943.
[11] M. B. Delghavi and A. Yazdani, "Sliding-mode control of AC voltages and currents of dispatchable distributed energy resources in master-slave-organized inverter-based microgrids," *IEEE Trans. Smart Grid*, vol. 10, no. 1, pp. 980–991, Jan. 2019.

[12] A. Bidram and A. Davoudi, "Hierarchical structure of microgrids control system," *IEEE Trans. Smart Grid*, vol. 3, no. 4, pp. 1963–1976, Dec. 2012.

[13] M. Raeispour, H. Atrianfar, H. R. Baghaee, and G. B. Gharehpetian, "Resilient H_∞ consensus-based control of autonomous AC microgrids with uncertain time-delayed communications," *IEEE Trans. Smart Grid*, vol. 11, no. 5, pp. 3871–3884, Sep. 2020.

[14] L. Meng, E. R. Sanseverino, A. Luna, T. Dragicevic, J. C. Vasquez, and J. M. Guerrero, "Microgrid supervisory controllers and energy management systems: A literature review," *Renew. Sustain. Energy Rev.*, vol. 60, pp. 1263–1273, Jul. 2016.

[15] O. Homaee, A. Zakariazadeh, and S. Jadid, "Retail market policy for distribution systems in presence of DERs and microgrids: Comparison of sequential and simultaneous settlement of energy and reactive power markets," *IET Gener., Transmiss. Distrib.*, vol. 14, no. 2, pp. 211–222, Jan. 2020.

[16] M. Raeispour, H. Atrianfar, H. R. Baghaee, and G. B. Gharehpetian, "Distributed LMI-based control of heterogeneous microgrids considering fixed time-delays and switching topologies," *IET Renew. Power Gener.*, vol. 14, no. 12, pp. 2068–2078, Mar. 2020.

[17] B. Abdolmaleki, Q. Shafiee, A. R. Seifi, M. M. Arefi, and F. Blaabjerg, "A zeno-free event-triggered secondary control for AC microgrids," *IEEE Trans. Smart Grid*, vol. 11, no. 3, pp. 1905–1916, May 2020.

[18] M. Raeispour, H. Atrianfar, H. R. Baghaee, and G. B. Gharehpetian, "Resilient distributed control of BESSs and voltage source converter-based microgrids considering switching topologies and non-uniform time-varying delays," *IET Gener., Transmiss. Distrib.*, vol. 14, no. 22, pp. 5060–5071, Oct. 2020.

[19] A. Afshari, M. Karrari, H. R. Baghaee, and G. B. Gharehpetian, "Resilient cooperative control of AC microgrids considering relative state-dependent noises andCommunication time-delays," *IET Renew. Power Gener.*, vol. 14, no. 8, pp. 1321–1331, Jun. 2020.

[20] M. Raeispour, H. Atrianfar, H. R. Baghaee, and G. B. Gharehpetian, "Robust distributed disturbance-resilient H_∞-based control of off-grid microgrids with uncertain communications," *IEEE Syst. J.*, vol. 15, no. 2, pp. 2895–2905, Jun. 2021.

[21] A. Afshari, M. Karrari, H. R. Baghaee, and G. B. Gharehpetian, "Resilient synchronization of voltage/frequency in AC microgrids under deception attacks," *IEEE Syst. J.*, vol. 15, no. 2, pp. 2125–2136, Jun. 2021.

[22] M. Aldeen and R. Sharma, "Robust detection of faults in frequency control loops," *IEEE Trans. Power Syst.*, vol. 22, no. 1, pp. 413–422, Feb. 2007.

[23] F. Caliskan and I. Genc, "A robust fault detection and isolation method in load frequency control loops," *IEEE Trans. Power Syst.*, vol. 23, no. 4, pp. 1756–1767, Nov. 2008.

[24] M. A. Shahab, B. Mozafari, S. Soleymani, N. M. Dehkordi, H. M. Shourkaei, and J. M. Guerrero, "Distributed consensus-based fault tolerant control of islanded microgrids," *IEEE Trans. Smart Grid*, vol. 11, no. 1, pp. 37–47, Jan. 2020.

[25] A. Afshari, M. Karrari, H. R. Baghaee, G. B. Gharehpetian, and S. Karrari, "Cooperative fault-tolerant control of microgrids under switching communication topology," *IEEE Trans. Smart Grid*, vol. 11, no. 3, pp. 1866–1879, May 2020.

[26] X. Li, Q. Xu, and F. Blaabjerg, "Adaptive resilient secondary control for islanded AC microgrids with sensor faults," *IEEE J. Emerg. Sel. Topics Power Electron.*, vol. 9, no. 5, pp. 5239–5248, Oct. 2021.

[27] N. M. Dehkordi and S. Z. Moussavi, "Distributed resilient adaptive control of islanded microgrids under sensor/actuator faults," *IEEE Trans. Smart Grid*, vol. 11, no. 3, pp. 2699–2708, May 2020.

[28] A. Afshari, M. Karrari, H. R. Baghaee, and G. B. Gharehpetian, "Distributed fault-tolerant voltage/frequency synchronization in autonomous AC microgrids," *IEEE Trans. Power Syst.*, vol. 35, no. 5, pp. 3774–3789, Sep. 2020.

[29] A. M. Shotorbani, S. Ghassem-Zadeh, B. Mohammadi-Ivatloo, and S. H. Hosseini, "A distributed secondary scheme with terminal sliding mode controller for energy storages in an islanded microgrid," *Int. J. Elect. Power Energy Syst.*, vol. 93, pp. 352–364, Dec. 2017.

[30] P. Lin and Y. Jia, "Average consensus in networks of multi-agents with both switching topology and coupling time-delay," *Phys. A, Stat. Mech. Appl.*, vol. 387, no. 1, pp. 303–313, Jan. 2008.

[31] Z. Li, Z. Duan, G. Chen, and L. Huang, "Consensus of multiagent systems and synchronization of complex networks: A unified viewpoint," *IEEE Trans. Circuits Syst. I, Reg. Papers*, vol. 57, no. 1, pp. 213–224, Jan. 2010.

[32] P. Massioni and M. Verhaegen, "Distributed control for identical dynamically coupled systems: A decomposition approach," *IEEE Trans. Autom. Control*, vol. 54, no. 1, pp. 124–135, Jan. 2009.

[33] M. Davoodi, N. Meskin, and K. Khorasani, "Simultaneous fault detection and consensus control design for a network of multi-agent systems," *Automatica*, vol. 66, no. 5, pp. 185–194, Apr. 2016.

[34] J. W. Simpson-Porco, Q. Shafiee, F. Dörfler, J. C. Vasquez, J. M. Guerrero, and F. Bullo, "Secondary frequency and voltage control of islanded microgrids via distributed averaging," *IEEE Trans. Ind. Electron.*, vol. 62, no. 11, pp. 7025–7038, Nov. 2015.

[35] A. Arancibia and K. Strunz, "Modeling of an electric vehicle charging station for fast DC charging," in *Proc. IEEE Int. Electr. Vehicle Conf.*, Mar. 2012, pp. 1–6.

[36] J. C. L. Chan and T. H. Lee, "Sliding mode observer-based fault-tolerant secondary control of microgrids," *Electronics*, vol. 9, no. 9, p. 1417, Sep. 2020.

[37] F. Guo, C. Wen, J. Mao, and Y. D. Song, "Distributed secondary voltage and frequency restoration control of droop-controlled inverter-based microgrids," *IEEE Trans. Ind. Electron.*, vol. 62, no. 7, pp. 4355–4364, Jul. 2015.

[38] G. Pipeleers, B. Demeulenaere, J. Swevers, and L. Vandenberghe, "Extended LMI characterizations for stability and performance of linear systems," *Syst. Control Lett.*, vol. 58, no. 7, pp. 510–518, 2009.

MOHAMMAD RAEISPOUR received the B.Sc. degree from the Qom University of Technology, Qom, Iran, in 2017, and the M.Sc. degree from the Amirkabir University of Technology, Tehran, Iran, in 2020, both in electrical and control engineering.

He is currently a Research Assistant with the Amirkabir University of Technology. His research interests include distributed coordination in multiagent systems, robust control, intelligent energy systems, modeling and advanced control of distribution systems and microgrids, and cyber-physical systems.

HAJAR ATRIANFAR (Member, IEEE) received the B.Sc. degree from Tehran University, Tehran, Iran, in 2002, and the M.Sc. and Ph.D. degrees from the Sharif University of Technology, Tehran, in 2004 and 2013, respectively, all in electrical engineering.

She is currently an Assistant Professor with the Amirkabir University of Technology. Her research interests include distributed coordination of multi-agent systems, cooperative robotics, cyber security in multi-agent systems, synchronization in smart grids, robust control, and nonlinear control theory.

MASOUD DAVARI (Senior Member, IEEE) was born in Isfahan, Iran, in September 1985. He received the B.Sc. degree (Hons.) in electrical engineering-power from the Isfahan University of Technology, Isfahan, in September 2007, the M.Sc. degree (Hons.) in electrical engineering-power from the Amirkabir University of Technology (Tehran Polytechnic), Tehran, Iran, in January 2010, and the Ph.D. degree in electrical engineering-energy systems from the University of Alberta, Edmonton, AB, Canada, in January 2016.

He was with the Iran Grid Secure Operation Research Center and the Iran's Electric Power Research Institute (EPRI), Tehran, from January 2010 to December 2011. From April 2015 to June 2017, he was collaborating with Quanta-Technology Company, Markham, ON, Canada, in the field of the dynamic interaction of renewable energy systems with smart grids, and control, protection, and automation of microgrids as a Senior Research and Development Specialist and a Senior Consultant. In July 2017, he joined the Department of Electrical and Computer Engineering in the Allen E. Paulson College of Engineering and Computing at Georgia Southern University, Statesboro, GA, USA, as a tenure-track Assistant Professor—where he was recommended and approved for being granted "*early*" promotion to Associate Professor and award of "*early*" tenure on December 3, 2021. He is currently the Founder and the Director of the Laboratory for Advanced Power and Energy Systems (LAPES), State-of-the-Art Center for Engineering and Research (CEaR) established in 2021 with Georgia Southern University. He has developed and implemented several experimental test rigs for both research universities and the industry. He has also authored several IEEE TRANSACTIONS and journals. His research interests include the dynamics, controls, and protections of different power electronic converters, which are utilized in the hybrid ac/dc smart grids, and hardware-in-the-loop (HIL) simulation-based testing of modernized power systems.

Dr. Davari has been serving as an Active Member and the Chapter Lead for the IEEE Power and Energy Society Task Force on Innovative Teaching Methods for Modern Power and Energy Systems since July 2020 and the Chapter 3 in the IEEE Working Group P2004, a newly established IEEE working group on the HIL simulation for IEEE Standards Association, since June 2017. He is also an Invited Member of the Golden Key International Honour Society. He was the Best Reviewer of the IEEE TRANSACTIONS ON POWER SYSTEMS in 2018 and 2020. He was a recipient of the 2019–2020 Allen E. Paulson College of Engineering and Computing (CEC) Faculty Award for Outstanding Scholarly Activity in the Allen E. Paulson CEC at Georgia Southern University and the winner of the Discovery & Innovation Award from the 2020–2021 University Awards of Excellence at Georgia Southern University. He served as the Chair for the Literature Review Subgroup of DC@Home Standards for the IEEE Standards Association from April 2014 to October 2015. He is also an invited reviewer of several of the IEEE TRANSACTIONS and journals, IET journals, *Energies* journal, and various IEEE conferences and an invited speaker at different universities and in diverse societies.

GEVORK B. GHAREHPETIAN (Senior Member, IEEE) received the B.Sc. degree (Hons.) from Tabriz University, Tabriz, Iran, in 1987, the M.Sc. degree (Hons.) from the Amirkabir University of Technology (AUT), Tehran, Iran, in 1989, and the Ph.D. degree (Hons.) from Tehran University, Tehran, in 1996, all in electrical engineering.

He was with the High Voltage Institute, RWTH Aachen, Aachen, Germany. He was holding an Assistant Professor position at AUT, from 1997 to 2003, and the position of an Associate Professor, from 2004 to 2007, and has been a Professor since 2007. Based on the Web of Science database (2005–2019), he is among World's Top 1% Elite Scientists according to Essential Science Indicators (ESI) ranking system. He is the author of more than 1200 journal and conference papers. His teaching and research interests include smart grids, microgrids, FACTS and HVDC systems, and monitoring of power transformers and their transient studies.

Dr. Gharehpetian received the Scholarship from the German Academic Exchange Service (DAAD) for his Ph.D. program, from 1993 to 1996. He was selected by the Ministry of Science Research and Technology (MSRT) as a Distinguished Professor of Iran in 2008, the Iranian Association of Electrical and Electronics Engineers (IAEEE) as a Distinguished Researcher of Iran in 2010, the Iran Energy Association (IEA) as the Best Researcher of Iran in the field of energy in 2018, the MSRT as a Distinguished Researcher of Iran in 2018, the Academy of Science of the Islamic Republic of Iran as a Distinguished Professor of electrical engineering in 2019, and the National Elites Foundation as the Laureates of Alameh Tabatabaei Award and was awarded the National Prize in 2019. Since 2004, he has been the Editor-in-Chief of the *Journal of IAEEE*. He is also a Distinguished Member of CIGRE and IAEEE.